

ENABLING AND INTERPRETING HYPER-DIFFERENTIAL SENSITIVITY ANALYSIS FOR BAYESIAN INVERSE PROBLEMS *

JOSEPH HART[†] AND BART VAN BLOEMEN WAANDERS[‡]

Abstract. Inverse problems constrained by partial differential equations (PDEs) play a critical role in model development and calibration. In many applications, there are multiple uncertain parameters in a model which must be estimated. Although the Bayesian formulation is attractive for such problems, computational cost and high dimensionality frequently prohibit a thorough exploration of the parametric uncertainty. A common approach is to reduce the dimension by fixing some parameters (which we will call auxiliary parameters) to a best estimate and using techniques from PDE-constrained optimization to approximate properties of the Bayesian posterior distribution. For instance, the maximum a posteriori probability (MAP) and the Laplace approximation of the posterior covariance can be computed. In this article, we propose using hyper-differential sensitivity analysis (HDSA) to assess the sensitivity of the MAP point to changes in the auxiliary parameters. We establish an interpretation of HDSA as correlations in the posterior distribution. Foundational assumptions for HDSA require satisfaction of the optimality conditions which are not always feasible or appropriate as a result of ill-posedness in the inverse problem. We introduce novel theoretical and computational approaches to justify and enable HDSA for ill-posed inverse problems by projecting the sensitivities on likelihood informed subspaces and defining a posteriori updates. Our proposed framework is demonstrated on a nonlinear multi-physics inverse problem motivated by estimation of spatially heterogeneous material properties in the presence of spatially distributed parametric modeling uncertainties.

Key words. Hyper-differential sensitivity analysis, Bayesian inverse problems, PDE-constrained optimization

AMS subject classifications. 65K10, 62F15

1. Introduction. Inverse problems are ubiquitous in scientific and engineering applications. They arise when a quantity cannot be directly observed but rather is estimated using observations of a related quantity. In the case of inverse problems constrained by partial differential equations (PDEs), the state variable (solution of the PDE) is observed at (potentially sparse) locations in space and/or instances in time, and from these observations one seeks to infer parameters in the model. There is a wealth of literature developing theory and computational methods to solve these challenging yet scientifically critical problems [5, 11, 26, 29]. Bayesian methods are attractive for their ability to assert prior knowledge and characterize uncertainty. However, for large-scale problems constrained by PDEs, there are a range of limitations which prohibit a complete Bayesian characterization of the uncertain parameters.

Among the many challenges faced in PDE-constrained inverse problems, data sparsity, high dimensionality, and computational complexity are at the forefront. It is common for PDE-based models of physical processes to have many uncertain param-

*Submitted to the editors DATE.

Funding: This paper describes objective technical results and analysis. Any subjective views or opinions that might be expressed in the paper do not necessarily represent the views of the U.S. Department of Energy or the United States Government. Sandia National Laboratories is a multimission laboratory managed and operated by National Technology and Engineering Solutions of Sandia LLC, a wholly owned subsidiary of Honeywell International, Inc., for the U.S. Department of Energy's National Nuclear Security Administration under contract DE-NA-0003525. SAND2021-6604 O.

[†]Optimization and Uncertainty Quantification, Sandia National Laboratories, P.O. Box 5800, Albuquerque, NM 87123-1320 (joshart@sandia.gov).

[‡]Optimization and Uncertainty Quantification, Sandia National Laboratories, P.O. Box 5800, Albuquerque, NM 87123-1320 (bartv@sandia.gov).

ters, some of which are spatially and/or temporally distributed. Ideally, one performs a statistical inversion such as applying a Markov Chain Monte Carlo sampler to explore the Bayesian posterior distribution for all of the uncertain parameters. However, such sampling is computationally prohibitive and hence simplifications are necessary. Two simplifications commonly employed in practice are to replace sampling with the solution of a PDE-constrained optimization problem and to fix some of the uncertain parameters to a best estimate which reduces the inverse problem dimension and improving numerical conditioning. Although pragmatic, these simplifications fail to adequately address underlying uncertainty.

This article considers the sensitivity of the inverse problem's solution due to perturbations in parameters that are fixed to a best estimate. These fixed parameters are sometimes called nuisance parameters in the inverse problems literature; however, in this article we adopt the term auxiliary parameters for greater generality. For problems with separable structure, variable projection may be used to write the parameter of interest as a function of the auxiliary parameters [3]. Alternatively, the error introduced by fixing auxiliary parameters to a nominal estimate may be represented in a Bayesian approximation error approach to incorporate their uncertainty in the inversion [21, 25]. This article presents hyper-differential sensitivity analysis (HDSA) as a tool to assess the influence of the auxiliary parameters on the maximum a posteriori probability point. Based on differentiating through optimality conditions, HDSA has been previously developed in the context of PDE-constrained optimization and shown to provide a computationally scalable approach to analyze uncertainty in large-scale optimization [16].

Connections between PDE-constrained optimization and Bayesian inverse problems are well established [5, 11, 26]. Nonetheless, HDSA, which is defined in the context of PDE-constrained optimization, has not been formally analyzed from a Bayesian perspective. We establish an interpretation of HDSA in the Bayesian context which extends the previous work from PDE-constrained optimization to Bayesian inversion. This perspective motivates the use and interpretation of HDSA as a valuable tool for uncertainty quantification in large-scale applications where the many model evaluations required by samplings based approaches are prohibitive.

Large-scale PDE-constrained inverse problems, even with the simplifying assumptions described above, are frequently ill-posed as a result of high dimensional parameter spaces and limited and noisy data. This ill-posedness creates theoretical and computational challenges for the HDSA framework [16] since it is build on the foundation of post-optimality sensitivity analysis [8, 13]. In particular, satisfaction of the first and second order optimality conditions is required for HDSA. However, such satisfaction may not be easily attained for many inverse problems where prior information is limited, nonlinearities are present, and limited computational resources are available. Failure to satisfy these assumptions prohibits the use of HDSA. This article introduces novel theoretical and computational approaches and thereby facilitating use of HDSA for ill-posed PDE-constrained inverse problems. Our contributions include:

- Establishing a Bayesian interpretation of HDSA which relates sensitivities to correlations in the posterior distribution, a critical characteristic to infer in high dimensional problems.
- Defining HDSA on likelihood informed subspaces and demonstrating its theoretical and computational advantages to combat ill-conditioning.
- Developing a posteriori updates to overcome the theoretical limitations of HDSA for ill-posed inverse problems.
- Providing an algorithmic framework to apply HDSA to ill-posed inverse prob-

lems and demonstrating its effectiveness on a nonlinear multi-physics application.

The article is organized as follows. Section 2 reviews Bayesian inverse problems and HDSA. The Bayesian interpretation of HDSA is established in Section 3 to formalize a statistical interpretation of the sensitivities. Practical challenges associated with high dimensionality and ill-conditioning prohibit the use of HDSA for ill-posed inverse problems. We introduce HDSA on likelihood informed subspaces and a posteriori updates in Section 4 to overcome these challenges. An algorithmic overview is presented in Section 5. We demonstrate our proposed approach on a multi-physics subsurface flow application in Section 6 which considers uncertainty in a permeability field, source, boundary conditions, and diffusion coefficient. Section 7 concludes the article with a perspective on how these developments aid large-scale inverse problems.

2. Background. We consider inverse problems to estimate parameters $z \in Z$, where Z may be finite or infinite dimensional. Assume that z may not be observed directly, but rather we have sparse and noisy observations of a state $u \in U$, where U is an appropriate function space, which is related to z by a PDE in the form

$$(2.1) \quad c(u, z, \theta) = 0$$

where $\theta \in \Theta$ are uncertain parameters, referred to as auxiliary parameters, needed to define the PDE.

Ideally, one may use the PDE (2.1) and observations of u to jointly invert for z and θ . In practice, this is challenging because z and θ are high (or infinite) dimensional and solving c requires significant computational effort. It is common to fix θ to a nominal estimate and invert only for z .

The contributions of this article apply to the finite dimensional inverse problem which arises from the discretization of the PDE. To simplify the exposition, we assume that $Z_h \subset Z$ and $\Theta_h \subset \Theta$ are finite dimensional (a result of the PDE discretization) with bases $\{y_1, y_2, \dots, y_m\} \subset Z_h$ and $\{\phi_1, \phi_2, \dots, \phi_n\} \subset \Theta_h$. We will use $\mathbf{z} = (z_1, z_2, \dots, z_m)^T \in \mathbb{R}^m$ and $\boldsymbol{\theta} = (\theta_1, \theta_2, \dots, \theta_n)^T \in \mathbb{R}^n$ to denote coordinate representations of elements in Z_h and Θ_h (which may be function spaces). Assume that the PDE is uniquely solvable for each $y \in Z_h$ and $\phi \in \Theta_h$ and let $\Psi : Z_h \times \Theta_h \rightarrow U$ denote the PDE solution operator, i.e.

$$c(\Psi(y, \phi), y, \phi) = 0 \quad \text{for all } y \in Z_h, \phi \in \Theta_h.$$

Let $F : \mathbb{R}^m \times \mathbb{R}^n \rightarrow \mathbb{R}^d$ denote the parameter-to-observable map for the discretized problem. Specifically,

$$F(\mathbf{z}, \boldsymbol{\theta}) = \mathcal{O} \left(\Psi \left(\sum_{i=1}^m z_i y_i, \sum_{i=1}^n \theta_i \phi_i \right) \right)$$

maps parameter coordinates $(\mathbf{z}, \boldsymbol{\theta})$ to observations of the PDE solution at d locations defined by the observation operator $\mathcal{O} : U \rightarrow \mathbb{R}^d$. Given data $\mathbf{d} \in \mathbb{R}^d$ and a nominal estimate $\boldsymbol{\theta}_{\text{prior}} \in \mathbb{R}^n$ (prior mean in a Bayesian formulation), the finite dimensional inverse problem is to determine \mathbf{z} such that

$$F(\mathbf{z}, \boldsymbol{\theta}_{\text{prior}}) \approx \mathbf{d}.$$

Inverse problems are frequently ill-posed in the sense that there are many different \mathbf{z} 's such that $F(\mathbf{z}, \boldsymbol{\theta}_{\text{prior}}) \approx \mathbf{d}$. This ill-posedness motivates a Bayesian formulation of the inverse problem which enables incorporation of prior knowledge and facilitates characterization of uncertainty.

2.1. Bayesian inverse problems. We formulate the Bayesian inverse problem assuming that the observed data \mathbf{d} has been contaminated with additive Gaussian noise with mean $\mathbf{0}$ and covariance $\Gamma_{\text{noise}} \in \mathbb{R}^{d \times d}$ and that the prior distribution for \mathbf{z} is Gaussian with mean $\mathbf{z}_{\text{prior}}$ and positive definite covariance $\Gamma_{\text{prior}} \in \mathbb{R}^{m \times m}$. Bayes' rule implies that π_{post} , the posterior probability density function (PDF) for \mathbf{z} given $\boldsymbol{\theta} = \boldsymbol{\theta}_{\text{prior}}$, is

$$\pi_{\text{post}}(\mathbf{z}|\boldsymbol{\theta}_{\text{prior}}) \propto \pi_{\text{like}}(\mathbf{d}|\mathbf{z}, \boldsymbol{\theta}_{\text{prior}})\pi_{\text{prior}}(\mathbf{z})$$

where

$$\pi_{\text{like}}(\mathbf{d}|\mathbf{z}, \boldsymbol{\theta}_{\text{prior}}) \propto \exp\left(-\frac{1}{2}(F(\mathbf{z}, \boldsymbol{\theta}_{\text{prior}}) - \mathbf{d})^T \Gamma_{\text{noise}}^{-1} (F(\mathbf{z}, \boldsymbol{\theta}_{\text{prior}}) - \mathbf{d})\right)$$

is the likelihood function and $\pi_{\text{prior}}(\mathbf{z})$ is the PDF for the prior distribution of \mathbf{z} . In general, $\pi_{\text{prior}}(\mathbf{z})$ may depend on $\boldsymbol{\theta}_{\text{prior}}$ but we omit the dependence for simplicity.

Observe that the local maxima of the posterior PDF are the local minima in the optimization problem

$$(2.2) \quad \min_{\mathbf{z} \in \mathbb{R}^m} J(\mathbf{z}; \boldsymbol{\theta}_{\text{prior}}) := M(\mathbf{z}, \boldsymbol{\theta}_{\text{prior}}) + R(\mathbf{z})$$

where

$$M(\mathbf{z}, \boldsymbol{\theta}_{\text{prior}}) = \frac{1}{2}(F(\mathbf{z}, \boldsymbol{\theta}_{\text{prior}}) - \mathbf{d})^T \Gamma_{\text{noise}}^{-1} (F(\mathbf{z}, \boldsymbol{\theta}_{\text{prior}}) - \mathbf{d})$$

is the negative log likelihood and

$$R(\mathbf{z}) = \frac{1}{2}(\mathbf{z} - \mathbf{z}_{\text{prior}})^T \Gamma_{\text{prior}}^{-1} (\mathbf{z} - \mathbf{z}_{\text{prior}})$$

is the negative log of the prior PDF (with normalizing constants omitted). In the context of the optimization problem (2.2), we will also refer to M and R as the misfit and regularization, respectively.

Local minima of (2.2) are referred to as maximum a posteriori probability (MAP) points and correspond to parameters of highest probability. For high dimensional inverse problems constrained by computationally intensive PDEs, sampling from the posterior distribution is challenging so estimating the MAP point(s), and possibly the posterior covariance, is a computationally advantageous alternative to provide partial characterization of the posterior distribution. When F is a linear function, the posterior distribution is Gaussian and its covariance matrix is given by the inverse Hessian of J [10]. For a general nonlinear F , the posterior covariance is more difficult to estimate. The Laplace approximation, a common approach in practice, takes a linear approximation of F around the MAP point so that the posterior covariance matrix is approximated by the inverse Hessian [20].

In practice, computing the MAP point (2.2) for large-scale inverse problems is computationally challenging since it requires many PDE solves [5, 11, 26]. However, techniques from PDE-constrained optimization may be leveraged to solve (2.2) at large-scales. We use techniques including finite element discretization, matrix free linear algebra, adjoint-based derivative computation, and parallel computing. The reader is referred to [2, 4–7, 9, 14, 17–19, 22, 23, 31, 32] for a sampling of the PDE-constrained optimization literature. From the perspective of the Bayesian inverse problem, PDE-constrained optimization is a valuable tool to efficiently compute the MAP point (and possibly approximate the covariance).

2.2. Hyper-differential sensitivity analysis. Through a combination of tools from post-optimality sensitivity analysis, PDE-constrained optimization, and numerical linear algebra, HDSA has provided unique and valuable insights for optimal control and deterministic inverse problems [16, 27, 30]. This subsection provides essential background to prepare for our extension of HDSA to Bayesian inverse problems which follows. To facilitate our analysis, assume that $J : \mathbb{R}^m \times \mathbb{R}^n \rightarrow \mathbb{R}$, the objective function in (2.2), is twice continuously differentiable with respect to $(\mathbf{z}, \boldsymbol{\theta})$.

Let \mathbf{z}^* be a local minimum of the MAP point estimation problem (2.2) with auxiliary parameters fixed to $\boldsymbol{\theta} = \boldsymbol{\theta}_{\text{prior}} \in \mathbb{R}^n$. A fundamental assumption of HDSA is that \mathbf{z}^* satisfies the well known first and second order optimality conditions:

- (A1) $\nabla_{\mathbf{z}} J(\mathbf{z}^*; \boldsymbol{\theta}_{\text{prior}}) = 0$,
- (A2) $\nabla_{\mathbf{z}, \mathbf{z}} J(\mathbf{z}^*; \boldsymbol{\theta}_{\text{prior}})$ is positive definite,

where $\nabla_{\mathbf{z}} J$ and $\nabla_{\mathbf{z}, \mathbf{z}} J$ denote the gradient and Hessian of J with respect to \mathbf{z} , respectively. Then the implicit function theorem gives the existence of a continuously differentiable operator $\mathcal{G} : \mathcal{N}(\boldsymbol{\theta}_{\text{prior}}) \rightarrow \mathbb{R}^m$, defined on a neighborhood of $\boldsymbol{\theta}_{\text{prior}}$, such that $\nabla_{\mathbf{z}} J(\mathcal{G}(\boldsymbol{\theta}); \boldsymbol{\theta}) = 0$ for all $\boldsymbol{\theta} \in \mathcal{N}(\boldsymbol{\theta}_{\text{prior}})$. Furthermore, the Jacobian of \mathcal{G} , evaluated at $\boldsymbol{\theta}_{\text{prior}}$, is given by

$$(2.3) \quad \mathcal{G}'(\boldsymbol{\theta}_{\text{prior}}) = -\mathcal{H}^{-1}\mathcal{B},$$

where $\mathcal{B} = \nabla_{\mathbf{z}, \boldsymbol{\theta}} J(\mathbf{z}^*, \boldsymbol{\theta}_{\text{prior}})$ denotes the Jacobian of $\nabla_{\mathbf{z}} J$ with respect to $\boldsymbol{\theta}$, and $\mathcal{H} = \nabla_{\mathbf{z}, \mathbf{z}} J(\mathbf{z}^*, \boldsymbol{\theta}_{\text{prior}})$ denotes the Hessian of J with respect to \mathbf{z} , each evaluated at $\mathbf{z} = \mathbf{z}^*$ and $\boldsymbol{\theta} = \boldsymbol{\theta}_{\text{prior}}$. Then we may interpret $\mathcal{G}'(\boldsymbol{\theta}_{\text{prior}})\bar{\boldsymbol{\theta}}$ as the change in the optimal solution of (2.2) when $\boldsymbol{\theta}_{\text{prior}}$ is perturbed in the direction $\bar{\boldsymbol{\theta}}$, i.e. the sensitivity of the MAP point \mathbf{z}^* to the perturbation $\bar{\boldsymbol{\theta}}$.

We may only be interested in the sensitivity of certain features of \mathbf{z}^* , for instance, those which are most informed by the data. To achieve this, we introduce a linear operator

$$\mathcal{P} : \mathbb{R}^m \rightarrow \mathbb{R}^m$$

which projects \mathbf{z}^* onto a subspace in which we seek to perform our analysis. In subsection 4.1, we propose to define \mathcal{P} using the likelihood informed subspace to combat ill-conditioning.

To associate sensitivity with each basis function $\phi_i \in \Theta_h$, we assume that $\|\phi_i\|_{\Theta} = 1$, $i = 1, 2, \dots, n$, and define the hyper-differential sensitivity indices

$$(2.4) \quad S_i = \|\mathcal{P}\mathcal{H}^{-1}\mathcal{B}\mathbf{e}_i\|_{W_Z} \quad i = 1, 2, \dots, n,$$

where $\mathbf{e}_i \in \mathbb{R}^m$ is the coordinate representation of the basis function ϕ_i . The norm $\|\cdot\|_{W_Z}$ is defined on coordinates in \mathbb{R}^m weighted by $W_Z \in \mathbb{R}^{m \times m}$, where $(W_Z)_{i,j} = (y_i, y_j)_Z$, so that the sensitivity indices magnitude may be understood in the native space Z . We interpret S_i as the change in the projected (on the range space of \mathcal{P}) MAP point, measured in Z , if the auxiliary parameters are perturbed in the direction ϕ_i . In Section 3, we establish a statistical interpretation of S_i in terms of local correlations.

We note that HDSA may be formally developed more generally for infinite dimensional problems in a full space optimization framework. The reader is directed to [16] for additional details.

3. Interpretation of HDSA for Bayesian inverse problems. Although HDSA was developed in the context of PDE-constrained optimization, linking it to the MAP point estimation problem establishes a statistical interpretation of the sensitivity indices. As previously highlighted, the inverse Hessian of J with respect to \mathbf{z}

equals the covariance matrix of the posterior distribution when F is linear [10], and is sometimes used to approximate the posterior covariance for nonlinear problems [20]. We follow a similar logic to establish an interpretation of HDSA as a correlation in the joint posterior distribution of $(\mathbf{z}, \boldsymbol{\theta})$. We provide an analytical result for linear inverse problems and then argue for its local validity in nonlinear inverse problems.

Consider the Bayesian inverse problem on the joint distribution of $(\mathbf{z}, \boldsymbol{\theta})$ and assume that the parameter-to-observable map $F(\mathbf{z}, \boldsymbol{\theta})$ is linear in $(\mathbf{z}, \boldsymbol{\theta})$, i.e. $F(\mathbf{z}, \boldsymbol{\theta}) = A\mathbf{z} + B\boldsymbol{\theta}$ for given matrices $A \in \mathbb{R}^{d \times m}$ and $B \in \mathbb{R}^{d \times n}$. Assuming a joint Gaussian prior on $(\mathbf{z}, \boldsymbol{\theta})$ with mean $(\mathbf{z}_{\text{prior}}, \boldsymbol{\theta}_{\text{prior}})$ and covariance matrix $\Pi_{\text{prior}} \in \mathbb{R}^{(m+n) \times (m+n)}$, the posterior distribution is Gaussian with its mean (corresponding to the unique MAP point) given by the solution of

$$\min_{\mathbf{z} \in \mathbb{R}^m, \boldsymbol{\theta} \in \mathbb{R}^n} J_{\text{joint}}(\mathbf{z}, \boldsymbol{\theta}) := M_{\text{joint}}(\mathbf{z}, \boldsymbol{\theta}) + R_{\text{joint}}(\mathbf{z}, \boldsymbol{\theta})$$

where

$$M_{\text{joint}}(\mathbf{z}, \boldsymbol{\theta}) = \frac{1}{2} (A\mathbf{z} + B\boldsymbol{\theta} - \mathbf{d})^T \Gamma_{\text{noise}}^{-1} (A\mathbf{z} + B\boldsymbol{\theta} - \mathbf{d})$$

and

$$R_{\text{joint}}(\mathbf{z}, \boldsymbol{\theta}) = \frac{1}{2} \begin{pmatrix} \mathbf{z} - \mathbf{z}_{\text{prior}} \\ \boldsymbol{\theta} - \boldsymbol{\theta}_{\text{prior}} \end{pmatrix}^T \Pi_{\text{prior}}^{-1} \begin{pmatrix} \mathbf{z} - \mathbf{z}_{\text{prior}} \\ \boldsymbol{\theta} - \boldsymbol{\theta}_{\text{prior}} \end{pmatrix}.$$

Further, its posterior covariance matrix

$$(3.1) \quad \Sigma_{\text{post}} = \begin{pmatrix} \Sigma_{\mathbf{z}, \mathbf{z}} & \Sigma_{\mathbf{z}, \boldsymbol{\theta}} \\ \Sigma_{\boldsymbol{\theta}, \mathbf{z}} & \Sigma_{\boldsymbol{\theta}, \boldsymbol{\theta}} \end{pmatrix}$$

is given by the inverse Hessian of J_{joint} , assuming it is invertible [10]. Theorem 3.1 provides an interpretation of HDSA in the context of the posterior covariance matrix (3.1).

THEOREM 3.1. *Assume that the Hessian of J_{joint} with respect to $(\mathbf{z}, \boldsymbol{\theta})$ is positive definite and \mathbf{z}^* is the minimum of $J_{\text{joint}}(\mathbf{z}, \boldsymbol{\theta}_{\text{prior}})$, where $\boldsymbol{\theta}_{\text{prior}}$ is the fixed nominal estimate. Then the sensitivity of the optimal \mathbf{z}^* with respect to perturbations of $\boldsymbol{\theta}_{\text{prior}}$, $\mathcal{G}'(\boldsymbol{\theta}_{\text{prior}})$ defined in (2.3), satisfies*

$$\mathcal{G}'(\boldsymbol{\theta}_{\text{prior}}) = \Sigma_{\mathbf{z}, \boldsymbol{\theta}} \Sigma_{\boldsymbol{\theta}, \boldsymbol{\theta}}^{-1}.$$

Proof. Algebraic manipulations of J_{joint} yields

$$J_{\text{joint}}(\mathbf{z}, \boldsymbol{\theta}) = \frac{1}{2} \mathbf{z}^T \Upsilon_{\mathbf{z}, \mathbf{z}} \mathbf{z} + \frac{1}{2} \boldsymbol{\theta}^T \Upsilon_{\boldsymbol{\theta}, \boldsymbol{\theta}} \boldsymbol{\theta} + \mathbf{z}^T \Upsilon_{\mathbf{z}, \boldsymbol{\theta}} \boldsymbol{\theta} - \mathbf{z}^T \boldsymbol{\gamma}_{\mathbf{z}} - \boldsymbol{\theta}^T \boldsymbol{\gamma}_{\boldsymbol{\theta}} + \beta$$

where

$$\Upsilon_{\mathbf{z}, \mathbf{z}} = A^T \Gamma_{\text{noise}}^{-1} A + C_{\mathbf{z}, \mathbf{z}} \quad \Upsilon_{\boldsymbol{\theta}, \boldsymbol{\theta}} = B^T \Gamma_{\text{noise}}^{-1} B + C_{\boldsymbol{\theta}, \boldsymbol{\theta}} \quad \Upsilon_{\mathbf{z}, \boldsymbol{\theta}} = A^T \Gamma_{\text{noise}}^{-1} B + C_{\mathbf{z}, \boldsymbol{\theta}}$$

$$\boldsymbol{\gamma}_{\mathbf{z}} = A^T \Gamma_{\text{noise}}^{-1} \mathbf{d} + C_{\mathbf{z}, \mathbf{z}} \mathbf{z}_{\text{prior}} + C_{\mathbf{z}, \boldsymbol{\theta}} \boldsymbol{\theta}_{\text{prior}} \quad \boldsymbol{\gamma}_{\boldsymbol{\theta}} = B^T \Gamma_{\text{noise}}^{-1} \mathbf{d} + C_{\boldsymbol{\theta}, \boldsymbol{\theta}} \boldsymbol{\theta}_{\text{prior}} + C_{\boldsymbol{\theta}, \mathbf{z}} \mathbf{z}_{\text{prior}}$$

$$\beta = \frac{1}{2} \mathbf{d}^T \Gamma_{\text{noise}}^{-1} \mathbf{d} + \frac{1}{2} \mathbf{z}_{\text{prior}}^T C_{\mathbf{z}, \mathbf{z}} \mathbf{z}_{\text{prior}} + \mathbf{z}_{\text{prior}}^T C_{\mathbf{z}, \boldsymbol{\theta}} \boldsymbol{\theta}_{\text{prior}} + \frac{1}{2} \boldsymbol{\theta}_{\text{prior}}^T C_{\boldsymbol{\theta}, \boldsymbol{\theta}} \boldsymbol{\theta}_{\text{prior}}$$

with $C_{z,z}$, $C_{z,\theta}$, $C_{\theta,z}$, and $C_{\theta,\theta}$ coming from Π_{prior}^{-1} , i.e.

$$\Pi_{\text{prior}}^{-1} = \begin{pmatrix} C_{z,z} & C_{z,\theta} \\ C_{\theta,z} & C_{\theta,\theta} \end{pmatrix}.$$

Computing derivatives as in subsection 2.2 yields $\mathcal{G}'(\boldsymbol{\theta}_{\text{prior}}) = -\Upsilon_{z,z}^{-1}\Upsilon_{z,\theta}$. Since the posterior covariance Σ is given by the inverse of the Hessian of J_{joint} , results from [24] and our assumption of positive definiteness of the Hessian yields

$$\Sigma_{z,\theta} = -\Upsilon_{z,z}^{-1}\Upsilon_{z,\theta}(\Upsilon_{\theta,\theta} - \Upsilon_{z,\theta}^T\Upsilon_{z,z}^{-1}\Upsilon_{z,\theta})^{-1}$$

and

$$\Sigma_{\theta,\theta} = (\Upsilon_{\theta,\theta} - \Upsilon_{z,\theta}^T\Upsilon_{z,z}^{-1}\Upsilon_{z,\theta})^{-1}.$$

Using these expressions we have

$$\begin{aligned} \Sigma_{z,\theta}\Sigma_{\theta,\theta}^{-1} &= -\Upsilon_{z,z}^{-1}\Upsilon_{z,\theta}(\Upsilon_{\theta,\theta} - \Upsilon_{z,\theta}^T\Upsilon_{z,z}^{-1}\Upsilon_{z,\theta})^{-1}((\Upsilon_{\theta,\theta} - \Upsilon_{z,\theta}^T\Upsilon_{z,z}^{-1}\Upsilon_{z,\theta})^{-1})^{-1} \\ &= -\Upsilon_{z,z}^{-1}\Upsilon_{z,\theta} \\ &= \mathcal{G}'(\boldsymbol{\theta}_{\text{prior}}) \end{aligned} \quad \square$$

Theorem 3.1 implies that the sensitivity of the MAP point for \mathbf{z} with respect to $\boldsymbol{\theta}$, for linear Bayesian inverse problems with Gaussian noise and priors, corresponds to the posterior covariance between \mathbf{z} and $\boldsymbol{\theta}$, scaled by the variance of $\boldsymbol{\theta}$. This provides a foundation to interpret HDSA in terms of the correlation between \mathbf{z} and $\boldsymbol{\theta}$ in their joint posterior distribution. Correlations are a considerable challenge in joint inversion, and hence this interpretation of HDSA provides critical posterior information to enable better characterization of uncertainty.

Following similar principles of the Laplace approximation [20], HDSA may be interpreted as local correlations in the joint posterior distribution for nonlinear inverse problems. We provide two different perspectives, one based on linearizing the parameter-to-observable map and the other on conditional distributions, which arrive at this conclusion.

As in [20], we consider a linear approximation of F around $(\mathbf{z}^*, \boldsymbol{\theta}_{\text{prior}})$, i.e. the linear inverse problem whose parameter-to-observable map is

$$F(\mathbf{z}^*, \boldsymbol{\theta}_{\text{prior}}) + F'_z(\mathbf{z}^*, \boldsymbol{\theta}_{\text{prior}})(\mathbf{z} - \mathbf{z}^*) + F'_\theta(\mathbf{z}^*, \boldsymbol{\theta}_{\text{prior}})(\boldsymbol{\theta} - \boldsymbol{\theta}_{\text{prior}}),$$

where F'_z and F'_θ denote the Jacobians of F . Applying Theorem 3.1 to this linearized problem, $\mathcal{G}'(\boldsymbol{\theta}_{\text{prior}})$ measures the correlation between \mathbf{z} and $\boldsymbol{\theta}$ in the region where the linear approximation is valid, i.e. $\mathcal{G}'(\boldsymbol{\theta}_{\text{prior}})$ measures the local correlation between \mathbf{z} and $\boldsymbol{\theta}$ in a neighborhood of $(\mathbf{z}^*, \boldsymbol{\theta}_{\text{prior}})$.

From the conditional distribution perspective, since $J(\mathbf{z}, \boldsymbol{\theta})$ is the negative log of the joint posterior PDF, the local minima of $J(\mathbf{z}, \boldsymbol{\theta}_{\text{prior}})$, with $\boldsymbol{\theta}_{\text{prior}}$ fixed, correspond to the MAP point(s) of the joint posterior distribution of $(\mathbf{z}, \boldsymbol{\theta})$, conditioned on $\boldsymbol{\theta} = \boldsymbol{\theta}_{\text{prior}}$. Then following the interpretation of HDSA from subsection 2.2, $\mathcal{G}'(\boldsymbol{\theta}_{\text{prior}})$ measures the change in the MAP point of the distribution of \mathbf{z} conditioned on $\boldsymbol{\theta}_{\text{prior}}$, with respect to perturbations of $\boldsymbol{\theta}_{\text{prior}}$, i.e. the local correlation between \mathbf{z} and $\boldsymbol{\theta}$ in the neighborhood around $(\mathbf{z}^*, \boldsymbol{\theta}_{\text{prior}})$.

Both of these perspectives conclude that HDSA may be interpreted as a local correlation in a neighborhood of $(\mathbf{z}^*, \boldsymbol{\theta}_{\text{prior}})$, where the size of the neighborhood is determined by the nonlinearity F . Example 3.2 demonstrates this by overlaying the posterior PDF with sensitivity indices.

EXAMPLE 3.2. To illustrate the relationship between HDSA and correlations in the joint posterior distribution, consider the synthetic model problem

$$F(z, \theta_1, \theta_2) = e^{\frac{1}{10}z\theta_1} + \theta_2.$$

We generate three data points by evaluating F at the “true” parameters $(z, \theta_1, \theta_2) = (5, 5, 1)$ and contaminate them with Gaussian noise. Taking a Gaussian prior with mean and covariance matrix

$$(\mathbf{z}_{\text{prior}}, \boldsymbol{\theta}_{\text{prior}}) = (5, 5, 1) \quad \Pi_{\text{prior}} = \begin{pmatrix} 5^2 & 0 & 0 \\ 0 & 2^2 & 0 \\ 0 & 0 & .2^2 \end{pmatrix},$$

respectively, we consider joint inversion on (z, θ_1, θ_2) . Figure 1 displays the posterior PDF of (z, θ_1, θ_2) conditioned on $\theta_2 = 1$ (left panel) and $\theta_1 = 5$ (right panel) with MAP points and hyper-differential sensitivities indicated by dots.

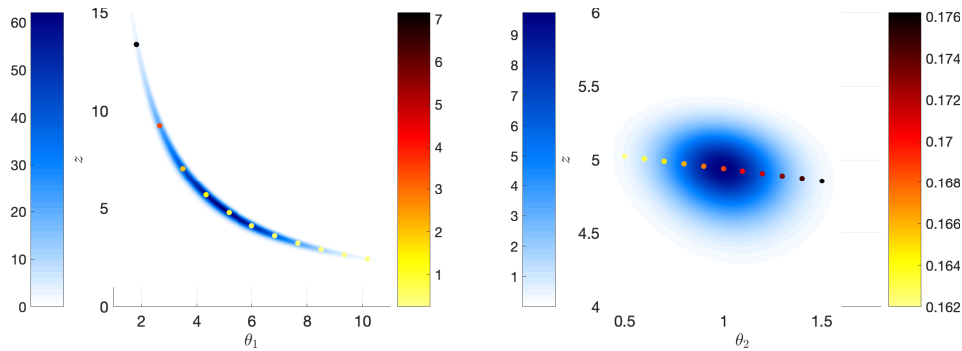


FIG. 1. Posterior PDF of (z, θ_1, θ_2) conditioned on $\theta_2 = 1$ (left panel) and $\theta_1 = 5$ (right panel). In each panel, the shading (in the blue color scale) indicates the PDF while the solid dots (in the red-yellow color scale) denote the maximum a posterior probability (MAP) point of the distribution of z conditioned on $\boldsymbol{\theta}$. The color of the dot (in the red-yellow color scale) indicates the hyper-differential sensitivity index for the MAP point with respect to θ_1 (left panel) and θ_2 (right panel).

We observe several trends which illustrate the interpretation of HDSA:

- The PDFs indicate a stronger dependency between z and θ_1 in comparison to z and θ_2 . Corresponding to this, we observe a much larger sensitivity index for θ_1 (given by the red-yellow color bar in the left panel) than θ_2 (given by the red-yellow color bar in the right panel).
- The sensitivity index varies with $\boldsymbol{\theta}$ showing that it is measuring local correlations which vary with $\boldsymbol{\theta}$. We observe the greatest sensitivity for small values of θ_1 which is consistent with the visual observation that the MAP point of the distribution of z conditioned on $\boldsymbol{\theta}$ varies more for small values of θ_1 .
- There is little variation in the sensitivities in the right panel where the distribution is approximately Gaussian (since local correlations do not vary in Gaussian distributions) and much greater variation in the left panel where the distribution is highly non-Gaussian.

4. Enabling HDSA for ill-posed inverse problems. For ill-posed inverse problems, it is frequently the case that a user does not solve the MAP point estimation problem (2.2) to optimality. The optimization routine may fail to produce a solution

which satisfies the first and/or second order optimality conditions, Assumptions (A1) and (A2), which are required in the formulation of HDSA. This lack of optimality occurs for a variety of interrelated reasons:

- The objective function J is flat in directions which are not well informed by the data and lack a strong prior to overcome this uncertainty.
- The Hessian is ill-conditioned since the directions along which the objective function is flat corresponds to small eigenvalues. Hence, numerical optimization schemes exhibit slow convergence around the local minimum as a result of error in second order information (for instance, error in the linear solve of a Newton step because of ill-conditioning).
- Solving to optimality (which is computationally intensive) is unnecessary when working with limited prior information. Characteristics of the MAP point in directions which are not well informed by the data and prior do not provide physically meaningful insights.

A common observation in practice is that the first few iterations of a numerical optimization routine is significantly informed by the data with a corresponding decrease in the objective function J , followed by potentially many time consuming iterations that produce small changes in the objective as the optimizers moves in the directions where J is flat. Hence, it is advantageous for a user to terminate the optimization routine prematurely yielding a z^* which fails to satisfy Assumption (A1) and possibly Assumption (A2).

These observations pose significant theoretical and numerical challenges when applying HDSA to ill-posed inverse problems. The assumptions required to define and interpret the operator \mathcal{G}' in (2.3) are not satisfied. This calls into question the theoretical validity of HDSA in this context and begs the question how it may be generalized. Furthermore, even if Assumptions (A1) and (A2) are satisfied, the numerical computation of \mathcal{G}' will be plagued by the ill-conditioning of the Hessian \mathcal{H} which must be inverted. In this section we propose a strategy to theoretically justify and numerically facilitate using HDSA in such problems.

We will first address the challenge of an ill-conditioned Hessian (assuming satisfaction of the optimality conditions) by projecting onto the likelihood informed subspace. Subsequently, we propose “a posteriori updates” which provide the theoretical foundation needed to justify HDSA when optimality conditions are not satisfied. In particular, we introduce first and second order updates when the optimality conditions, Assumptions (A1) and (A2), are not satisfied. We demonstrate that these updates introduce negligible computational overhead and the resulting inferences are robust to perturbations of the updates. Example 4.8 illustrates our developments on a synthetic prototype.

4.1. Projection on the likelihood informed subspace. Assume that the MAP point estimation problem (2.2) has been solved to optimality, but that the Hessian evaluated at the optimal solution, \mathcal{H} , is ill-conditioned. This ill conditioning coincides with directions which are poorly informed by both the data and prior. Changes in the optimal solution along these uninformed directions may not provide useful sensitivity information. Additionally, computing the sensitivity of these uninformed directions will be plagued by numerical challenges. This motivates us to define a projector, \mathcal{P} as introduced in subsection 2.2, onto the likelihood informed subspace (LIS) [12].

The LIS was considered in [12] for dimension reduction in nonlinear Bayesian inverse problems. It defines the informed directions (whose span defines the informed

subspace) as those given by r leading eigenvectors (corresponding to the largest eigenvalues) of the generalized eigenvalue problem

$$(4.1) \quad \mathcal{H}_M \mathbf{v}_j = \lambda_j \mathcal{H}_R \mathbf{v}_j, \quad j = 1, 2, \dots, r,$$

where

$$\mathcal{H}_M = \nabla_{\mathbf{z}, \mathbf{z}}^2 M(\mathbf{z}^*, \boldsymbol{\theta}_{\text{prior}})$$

is the misfit (or negative log likelihood) Hessian and

$$\mathcal{H}_R = \nabla_{\mathbf{z}, \mathbf{z}}^2 R(\mathbf{z}^*)$$

is the regularization (or negative log prior) Hessian. These dominant eigenvectors coincide with the directions in parameter space which are informed by the likelihood more than the prior. This may be observed by multiplying (4.1) by \mathbf{v}_j^T and solving for the Rayleigh quotient

$$(4.2) \quad \lambda_j = \frac{\mathbf{v}_j^T \mathcal{H}_M \mathbf{v}_j}{\mathbf{v}_j^T \mathcal{H}_R \mathbf{v}_j}, \quad j = 1, 2, \dots, r.$$

The eigenvalues measure the ratio of contributions from the likelihood and prior in the directions of the eigenvectors.

We define the projector

$$(4.3) \quad \mathcal{P} = \mathcal{V} \mathcal{V}^T \mathcal{H}_R$$

where the columns of $\mathcal{V} = [\mathbf{v}_1, \mathbf{v}_2, \dots, \mathbf{v}_r]$ are the eigenvectors of (4.1) normalized so that $\mathbf{v}_j^T \mathcal{H}_R \mathbf{v}_j = 1$, $j = 1, 2, \dots, r$. This corresponds to computing hyper-differential sensitivities in the directions which are informed more by the likelihood rather than the prior. The user must specify r ; however, the interpretation of the eigenvalues may be leveraged for this choice. For ill-posed inverse problems, r is typically small as a result of data sparsity and dissipative physics. In such case, the eigenvalues and eigenvectors may be efficiently computed using Krylov based methods or randomized solvers. Computational considerations are given in Section 5.

If the hyper-differential sensitivity indices (2.4) are computed directly using this definition of \mathcal{P} , it is necessary to invert the Hessian \mathcal{H} and apply \mathcal{P} to the resulting vector $\mathcal{H}^{-1} \mathcal{B} \boldsymbol{\theta}$, which poses a significant numerical challenge due to the ill-conditioning of \mathcal{H} . It is desirable to only compute the action of \mathcal{H}^{-1} in the subspace defined by the range of \mathcal{P} . Theorem 4.1 provides an expression for the sensitivity indices which only depends on the r leading generalized eigenvalues and eigenvectors in (4.1), rather than \mathcal{H}^{-1} . This shifts the computational burden from repeatedly inverting \mathcal{H} to computing the leading generalized eigenvalues and eigenvectors of (4.1) once, which is computationally advantageous for ill-posed inverse problems.

THEOREM 4.1. *If \mathcal{H} is positive definite then the LIS-hyper-differential sensitivities S_i , $i = 1, 2, \dots, n$, (where \mathcal{P} is defined by (4.3)) are given by*

$$(4.4) \quad S_i = \|\mathcal{P} \mathcal{H}^{-1} \mathcal{B} \mathbf{e}_i\|_{W_Z} = \sqrt{\sum_{k=1}^r \sum_{j=1}^r \left(\frac{\mathbf{v}_j^T \mathcal{B} \mathbf{e}_i}{1 + \lambda_j} \right) \left(\frac{\mathbf{v}_k^T \mathcal{B} \mathbf{e}_i}{1 + \lambda_k} \right) \mathbf{v}_k^T W_Z \mathbf{v}_j}.$$

Proof. Let $\{\lambda_j, \mathbf{v}_j\}_{j=1}^m$ denote the eigenvalues and (\mathcal{H}_R orthonormal) eigenvectors of (4.1). Then using the spectral representation of \mathcal{H}_M we have

$$\mathcal{H} = \sum_{j=1}^m \lambda_j \mathcal{H}_R \mathbf{v}_j \mathbf{v}_j^T \mathcal{H}_R + \mathcal{H}_R$$

and by the Sherman-Morrison-Woodbury formula we have

$$\mathcal{H}^{-1} = \mathcal{H}_R^{-1} - \sum_{j=1}^m \frac{\lambda_j}{1 + \lambda_j} \mathbf{v}_j \mathbf{v}_j^T.$$

Noting that $\mathcal{P}\mathbf{v}_k = \mathbf{v}_k$ for $k = 1, 2, \dots, r$ and $\mathcal{P}\mathbf{v}_k = 0$ for $k = r + 1, r + 2, \dots, m$, we have

$$S_i = \left\| \mathcal{P} \left(\mathcal{H}_R^{-1} - \sum_{i=1}^m \frac{\lambda_i}{1 + \lambda_i} \mathbf{v}_i \mathbf{v}_i^T \right) \mathcal{B} \mathbf{e}_i \right\|_{W_Z} = \left\| \sum_{j=1}^r \frac{1}{1 + \lambda_j} \mathbf{v}_j (\mathbf{v}_j^T \mathcal{B} \mathbf{e}_i) \right\|_{W_Z}.$$

Expressing the W_Z norm as the square root of the W_Z inner product, i.e. $\|\cdot\|_{W_Z} = \sqrt{(\cdot, \cdot)_{W_Z}}$, and manipulating algebra completes the proof. \square

4.2. First order a posteriori update. Assume that an optimization routine has been used to solve the MAP point estimation problem (2.2) and was terminated before convergence. Let \mathbf{z}^* be the solution obtained from the optimization routine for which $\nabla_{\mathbf{z}} J(\mathbf{z}^*; \boldsymbol{\theta}_{\text{prior}}) \neq 0$. If \mathcal{H} is invertible, one may compute the expression for the sensitivity indices (2.4); however, the interpretation and practical value of this quantity is questionable given that a fundamental assumption has been violated.

To facilitate HDSA we propose to “update” the objective function so that \mathbf{z}^* is a local minimum of the updated objective. This is reasonable given our previous assertions that the directions with a nonzero gradient are poorly informed by the data and prior. This update corresponds to perturbing the prior; however, we show that the HDSA results are robust to the prior perturbation since we project onto the likelihood informed subspace. In other words, the lack of theoretical validity arising from failure to meet optimality conditions is alleviated when sub-optimality occurs in uninformed directions.

Consider an additive update to the regularization (replacing R with $R + \tilde{R}$). To facilitate our analysis, we require that \tilde{R} to be quadratic, convex, and non-negative, which results in a perturbed Gaussian prior. We desire a minimum norm function for which \mathbf{z}^* is a stationary point of the updated objective $\tilde{J} := J + \tilde{R}$. Given these requirements, we define the set of candidate updates

$$Q = \{\tilde{R} : \mathbb{R}^m \rightarrow \mathbb{R} | \tilde{R} \geq 0, \tilde{R} \text{ is quadratic, } \tilde{R} \text{ is convex}\}$$

and pose the optimization problem

$$(4.5) \quad \begin{aligned} & \min_{\tilde{R} \in Q} \|\tilde{R}\|_{L^1(\mu)} \\ & \text{s.t. } \nabla_{\mathbf{z}} \tilde{R}(\mathbf{z}^*) = -\nabla_{\mathbf{z}} J(\mathbf{z}^*; \boldsymbol{\theta}_{\text{prior}}) \end{aligned}$$

where the norm $\|\tilde{R}\|_{L^1(\mu)}$ is the L^1 norm with respect to a Gaussian measure μ with mean \mathbf{z}^* and covariance matrix $\alpha^2 I$. This choice of norm emphasizes the size of \tilde{R}

around the solution \mathbf{z}^* with weighting from the covariance matrix $\alpha^2 I$ having length scale α in all directions. We assume \mathbf{z} has been scaled appropriately and define α as one half the distance between the maximum and minimum values in \mathbf{z}^* . Taking small values of α results in only considering characteristics of \tilde{R} in a small neighborhood of \mathbf{z}^* while taking very large values of α results in finding an update \tilde{R} which is very flat (nearly a constant function). Later in the article (Theorem 4.5) we will revisit the choice of α and show that our proposed framework is robust with respect to perturbations of α . More general measures and norms on \tilde{R} may be considered; however, this L^1 norm with a Gaussian measure is preferred because of its clear interpretation and amenability for analysis.

To enable computational efficiency and rigorous analysis, a closed form solution of (4.5) is given by Theorem 4.2.

THEOREM 4.2. *The global minimizer of (4.5) is given by*

$$(4.6) \quad \tilde{R}(\mathbf{z}) = \frac{\alpha}{2} \|\mathbf{g}\|_2 - (\mathbf{z} - \mathbf{z}^*)^T \mathbf{g} + \frac{1}{2} (\mathbf{z} - \mathbf{z}^*)^T \frac{1}{\alpha \|\mathbf{g}\|_2} \mathbf{g} \mathbf{g}^T (\mathbf{z} - \mathbf{z}^*),$$

where $\mathbf{g} = \nabla_{\mathbf{z}} J(\mathbf{z}^*; \boldsymbol{\theta}_{\text{prior}}) \neq 0$ is the gradient of J evaluated at \mathbf{z}^* and $\boldsymbol{\theta}_{\text{prior}}$.

Proof. We provide a sketch of the proof and refer the reader to the Appendix for additional details.

- 1 *Constraining the form of \tilde{R} :* Since $\tilde{R} \in Q$ and $\nabla_{\mathbf{z}} \tilde{R}(\mathbf{z}^*) = -\nabla_{\mathbf{z}} J(\mathbf{z}^*; \boldsymbol{\theta}_{\text{prior}})$ we may write it as a second degree Taylor polynomial centered at \mathbf{z}^* ,

$$\tilde{R}(\mathbf{z}) = C - \nabla_{\mathbf{z}} J(\mathbf{z}^*; \boldsymbol{\theta}_{\text{prior}})^T (\mathbf{z} - \mathbf{z}^*) + \frac{1}{2} (\mathbf{z} - \mathbf{z}^*)^T \mathcal{A} (\mathbf{z} - \mathbf{z}^*).$$

- 2 *Determining the constant term C :* Using the constraints $\tilde{R} \geq 0$ and \tilde{R} is convex, we may write C as a function of the \mathcal{A} to ensure non-negativity. Thus the optimization problem simplifies to finding a positive semidefinite matrix \mathcal{A} to define the quadratic term.
- 3 *Rewriting the objective:* Leveraging properties of gaussian distributions (the measure μ), the spectral decomposition of \mathcal{A} , and the L^1 norm with the non-negativity of \tilde{R} , we express the objective $\|\tilde{R}\|_{L^1(\mu)}$ as a function of the eigenvalues and eigenvectors of \mathcal{A} .
- 4 *Optimizing \mathcal{A} :* Using a sequence of lemmas, optimality assumptions and linear algebra properties are exploited to determine the form of \mathcal{A} which minimizes the objective $\|\tilde{R}\|_{L^1(\mu)}$. \square

The form (4.6) of the optimal update \tilde{R} is unsurprising in that its Hessian is proportional to the outer product of the nonzero gradient with itself, ensuring positive curvature in the gradient direction while having zero curvature in all other directions. The following observations demonstrate that \tilde{R} is well behaved as a function in the sense that it does not vary rapidly and \mathbf{z}^* is not one of its minima (i.e. it is not overfitting):

- $\tilde{R}(\mathbf{z}^*) = \frac{\alpha}{2} \|\mathbf{g}\|_2$.
- \tilde{R} attains its global minima at $\mathbf{z}^* + \alpha \frac{\mathbf{g}}{\|\mathbf{g}\|_2} + \mathbf{u}$ where $(\mathbf{u}, \mathbf{g})_2 = 0$.
- The 2-norm of the Hessian of \tilde{R} , denoted by $\mathcal{H}_{\tilde{R}}$, is given by $\|\mathcal{H}_{\tilde{R}}\|_2 = \|\mathbf{g}\|_2 / \alpha$.
- The norm of \tilde{R} is given by $\|\tilde{R}\|_{L^1(\mu)} = \alpha \|\mathbf{g}\|_2$.
- The maximum of \tilde{R} in a size α ball around \mathbf{z}^* is $2\alpha \|\mathbf{g}\|_2$.

Recalling that $R(\mathbf{z}, \boldsymbol{\theta}_{\text{prior}})$ is the negative log of a Gaussian prior PDF with mean $\mathbf{z}_{\text{prior}}$ and covariance Γ_{prior} , Theorem 4.3 identifies the updated regularization $R + \tilde{R}$ as corresponding to an updated Gaussian prior.

THEOREM 4.3. *The updated regularization $R + \tilde{R}$ is the negative log PDF (up to addition of a constant) of a Gaussian distribution with mean*

$$\tilde{\mathbf{z}}_{\text{prior}} = \mathbf{z}_{\text{prior}} + \frac{\alpha - (\mathbf{z}^* - \mathbf{z}_{\text{prior}})^T \mathbf{s}}{\alpha - \mathbf{v}^T \mathbf{s}} \mathbf{v}$$

and covariance

$$\tilde{\Gamma}_{\text{prior}} = \Gamma_{\text{prior}} - \frac{1}{\|\mathbf{g}\|_2} \frac{\mathbf{v} \mathbf{v}^T}{\alpha - \mathbf{v}^T \mathbf{s}}$$

where

$$\mathbf{g} = \nabla_{\mathbf{z}} J(\mathbf{z}^*; \boldsymbol{\theta}_{\text{prior}}), \quad \mathbf{s} = -\frac{\mathbf{g}}{\|\mathbf{g}\|_2}, \quad \text{and} \quad \mathbf{v} = \Gamma_{\text{prior}} \mathbf{g}.$$

Proof. Expanding products and collecting like terms, we can write

$$R(\mathbf{z}) + \tilde{R}(\mathbf{z}) = \frac{1}{2} \mathbf{z}^T \mathcal{Q} \mathbf{z} - \mathbf{z}^T \boldsymbol{\ell} + c$$

where

$$\mathcal{Q} = \Gamma_{\text{prior}}^{-1} + \frac{1}{\alpha \|\mathbf{g}\|_2} \mathbf{g} \mathbf{g}^T \quad \text{and} \quad \boldsymbol{\ell} = \Gamma_{\text{prior}}^{-1} \mathbf{z}_{\text{prior}} + \frac{1}{\alpha \|\mathbf{g}\|_2} \mathbf{g} \mathbf{g}^T \mathbf{z}^* + \mathbf{g}$$

and c is a constant. Completing the square, we may rewrite this as

$$R(\mathbf{z}) + \tilde{R}(\mathbf{z}) = \frac{1}{2} (\mathbf{z} - \mathcal{Q}^{-1} \boldsymbol{\ell})^T \mathcal{Q} (\mathbf{z} - \mathcal{Q}^{-1} \boldsymbol{\ell}) + c - \frac{1}{2} \boldsymbol{\ell}^T \mathcal{Q}^{-1} \boldsymbol{\ell}.$$

Then, up to addition of a constant, $R(\mathbf{z}) + \tilde{R}(\mathbf{z})$ is the negative log PDF for a Gaussian distribution with mean $\mathcal{Q}^{-1} \boldsymbol{\ell}$ and covariance \mathcal{Q}^{-1} . The resulting expressions for \mathcal{Q}^{-1} and $\mathcal{Q}^{-1} \boldsymbol{\ell}$ follow from the Sherman-Morrison formula and algebraic manipulations. Positive definiteness of the covariance matrix follows from the observation that \mathcal{Q} is the sum of two positive definite matrices and hence is itself positive definite. \square

Theorem 4.3 demonstrates the Bayesian interpretation of the first order update. The updated prior mean is shifted in the direction of $\mathbf{v} = \Gamma_{\text{prior}} \mathbf{g}$ (the nonzero gradient scaled by the prior covariance). The updated prior covariance corresponds to reducing the prior uncertainty in the direction \mathbf{v} since

$$\mathbf{v}^T \left(-\frac{1}{\|\mathbf{g}\|_2} \frac{\mathbf{v} \mathbf{v}^T}{\alpha - \mathbf{v}^T \mathbf{s}} \right) \mathbf{v} = -\frac{(\mathbf{v}^T \mathbf{v})^2}{\alpha \|\mathbf{g}\| + \mathbf{g}^T \Gamma_{\text{prior}} \mathbf{g}} < 0.$$

Hence, the updated prior ensures that \mathbf{z}^* is a MAP point by enforcing a stronger prior in the nonzero gradient direction.

By adding \tilde{R} , we define the perturbed MAP point estimation problem

$$(4.7) \quad \min_{\mathbf{z} \in \mathbb{R}^m} \tilde{J}(\mathbf{z}; \boldsymbol{\theta}) := J(\mathbf{z}; \boldsymbol{\theta}) + \tilde{R}(\mathbf{z}),$$

for which \mathbf{z}^* is a local minima when $\boldsymbol{\theta} = \boldsymbol{\theta}_{\text{prior}}$. Assuming that $\nabla_{\mathbf{z}, \mathbf{z}} \tilde{J}(\mathbf{z}^*; \boldsymbol{\theta}_{\text{prior}})$ is positive definite (subsection 4.3 considers when it is not), we may compute and

interpret hyper-differential sensitivity indices for the perturbed inverse problem whose MAP point is given by the solution of (4.7).

It is possible to compute ‘‘sensitivities’’ (which are not theoretically justified) using (2.4) or (4.4) for the original MAP point estimation problem (2.2) despite failures to meet optimality conditions. This raises the question: if sensitivity indices are computed for the original problem ignoring the fact that the gradient norm is nonzero, how much will they differ from the sensitivity indices computed for the perturbed problem (4.7), which are theoretically sound? Theorem 4.4 answers this question.

THEOREM 4.4. *Let \mathcal{H} and $\tilde{\mathcal{H}}$ denote the Hessian of J and \tilde{J} with respect to \mathbf{z} , evaluated at \mathbf{z}^* and $\boldsymbol{\theta}_{\text{prior}}$, respectively, and \mathcal{B} and $\tilde{\mathcal{B}}$ denote the Jacobian of $\nabla_{\mathbf{z}}J$ and $\nabla_{\mathbf{z}}\tilde{J}$, with respect to $\boldsymbol{\theta}$, evaluated at \mathbf{z}^* and $\boldsymbol{\theta}_{\text{prior}}$, respectively. Assuming that \mathcal{H} is positive definite, the quantities*

$$S_i = \|\mathcal{P}\mathcal{H}^{-1}\mathcal{B}\mathbf{e}_i\|_{W_Z} \quad \text{and} \quad \tilde{S}_i = \|\mathcal{P}\tilde{\mathcal{H}}^{-1}\tilde{\mathcal{B}}\mathbf{e}_i\|_{W_Z} \quad i = 1, 2, \dots, n,$$

satisfy

$$\frac{|\tilde{S}_i - S_i|}{\|\mathcal{H}^{-1}\mathcal{B}\mathbf{e}_i\|_{W_Z}} \leq \frac{\|\mathcal{P}\mathbf{n}\|_{W_Z}}{\mathbf{s}^T\mathbf{n} + \alpha},$$

where

$$\mathbf{g} = \nabla_{\mathbf{z}}J(\mathbf{z}^*; \boldsymbol{\theta}_{\text{prior}}), \quad \mathbf{s} = -\frac{\mathbf{g}}{\|\mathbf{g}\|_2}, \quad \text{and} \quad \mathbf{n} = -\mathcal{H}^{-1}\mathbf{g}.$$

Proof. First observe that $\tilde{\mathcal{B}} = \mathcal{B}$ since $\tilde{J} = J + \tilde{R}$ and \tilde{R} does not depend on $\boldsymbol{\theta}$. Hence,

$$\tilde{S}_i = \|\mathcal{P}(\mathcal{H} + \mathcal{H}_{\tilde{R}})^{-1}\mathcal{B}\mathbf{e}_i\|_{W_Z} \quad \text{and} \quad S_i = \|\mathcal{P}\mathcal{H}^{-1}\mathcal{B}\mathbf{e}_i\|_{W_Z},$$

where $\mathcal{H}_{\tilde{R}} = \mathbf{g}\mathbf{g}^T/(\alpha\|\mathbf{g}\|_2)$ is the Hessian of \tilde{R} .

Applying the reverse triangle inequality yields

$$|\tilde{S}_i - S_i| \leq \|\mathcal{P}((\mathcal{H} + \mathcal{H}_{\tilde{R}})^{-1}\mathcal{B}\mathbf{e}_i - \mathcal{H}^{-1}\mathcal{B}\mathbf{e}_i)\|_{W_Z}.$$

Using the Sherman-Morrison formula for rank one updates and properties of norms we have

$$\begin{aligned} |\tilde{S}_i - S_i| &\leq \left\| \mathcal{P} \frac{1}{1 + \frac{\|\mathbf{g}\|_2}{\alpha} \mathbf{s}^T \mathcal{H}^{-1} \mathbf{s}} \mathcal{H}^{-1} \mathcal{H}_{\tilde{R}} \mathcal{H}^{-1} \mathcal{B}\mathbf{e}_i \right\|_{W_Z} \\ &\leq \frac{1}{1 + \frac{\|\mathbf{g}\|_2}{\alpha} \mathbf{s}^T \mathcal{H}^{-1} \mathbf{s}} \cdot \|\mathcal{P}\mathcal{H}^{-1}\mathcal{H}_{\tilde{R}}\|_{W_Z} \cdot \|\mathcal{H}^{-1}\mathcal{B}\mathbf{e}_i\|_{W_Z} \end{aligned}$$

Dividing by $\|\mathcal{H}^{-1}\mathcal{B}\mathbf{e}_i\|_{W_Z}$, plugging in $\mathcal{H}_{\tilde{R}} = \mathbf{g}\mathbf{g}^T/(\alpha\|\mathbf{g}\|_2)$, and manipulating constants yields

$$(4.8) \quad \frac{|\tilde{S}_i - S_i|}{\|\mathcal{H}^{-1}\mathcal{B}\mathbf{e}_i\|_{W_Z}} \leq \frac{\|\mathbf{g}\|_2}{\alpha + \mathbf{s}^T\mathbf{n}} \|\mathcal{P}\mathcal{H}^{-1}\mathbf{s}\mathbf{s}^T\|_{W_Z}.$$

Notice that $\|\mathcal{P}\mathcal{H}^{-1}\mathbf{s}\mathbf{s}^T\|_{W_Z} = \|\mathcal{P}\mathcal{H}^{-1}\mathbf{s}\|_{W_Z}$ since it is a rank one matrix given by the outer product of $\mathcal{P}\mathcal{H}^{-1}\mathbf{s}$ and \mathbf{s} with $\|\mathbf{s}\|_2 = 1$. Plugging this into (4.8) and manipulating constants completes the proof. \square

Conceptually, Theorem 4.4 indicates that the relative difference between the i^{th} sensitivity index for perturbed and original MAP point estimation problems is given by the size of the projection of the Newton step $\mathcal{P}\mathbf{n}$ in the next optimization iterate, divided by the portion of the Newton step pointing in the negative gradient direction plus the length scale parameter α . Hence if \mathbf{z}^* is optimized in the subspace defined by the range of \mathcal{P} (the likelihood informed subspace), then $\|\mathcal{P}\mathbf{n}\|_{W_Z}$ will be small implying that the difference between the theoretically justified sensitivity indices for the perturbed MAP point estimation problem and the ill-defined ‘‘sensitivity indices’’ for the original MAP point estimation problem will be small. We may compute $\|\mathcal{P}\mathbf{n}\|_{W_Z}$ using the eigenvalues and eigenvectors defining the LIS to confirm its magnitude in practice. For the permeability inversion problem in Section 6 we have $\|\mathcal{P}\mathbf{n}\|_{W_Z} = \mathcal{O}(10^{-4})$. Prior to developing the first order update we had no justification for applying HDSA to the MAP point estimation problem (2.2) with sub-optimal solutions; however, our formulation of \tilde{R} and Theorems 4.3 and 4.4 provides the theoretical insights needed to properly define and interpret hyper-differential sensitivity indices for suboptimal solutions.

The length scale parameter α defining \tilde{R} appears throughout our analysis. Theorem 4.5 below establishes our previous assertion that the sensitivity indices are robust with respect to changes in α .

THEOREM 4.5. *Let $\tilde{\mathcal{H}}(\alpha)$ denote the Hessian of \tilde{J} with respect to \mathbf{z} and $\tilde{\mathcal{B}}(\alpha)$ denote the Jacobian of $\nabla_{\mathbf{z}}\tilde{J}$ with respect to $\boldsymbol{\theta}$, each evaluated at \mathbf{z}^* and $\boldsymbol{\theta}_{\text{prior}}$, and considered as functions of α . Letting $\tilde{S}_i(\alpha)$ be the sensitivity index defined by (4.4), as a function of α , and assuming that \mathcal{H} is positive definite we have*

$$\frac{|\tilde{S}_i(\alpha + \alpha\beta) - \tilde{S}_i(\alpha)|}{\|\mathcal{H}^{-1}\mathcal{B}\mathbf{e}_i\|_{W_Z}} < |\beta| \cdot \frac{\|\mathcal{P}\mathbf{n}\|_{W_Z}}{\mathbf{s}^T\mathbf{n} + \alpha(1 + \beta)} \quad \text{for } -1 < \beta < 1$$

where

$$\mathbf{g} = \nabla_{\mathbf{z}}J(\mathbf{z}^*; \boldsymbol{\theta}_{\text{prior}}), \quad \mathbf{s} = -\frac{\mathbf{g}}{\|\mathbf{g}\|_2}, \quad \text{and} \quad \mathbf{n} = -\mathcal{H}^{-1}\mathbf{g}.$$

Proof. Noting that $\tilde{\mathcal{B}}(\alpha)\mathbf{e}_i = \tilde{\mathcal{B}}(\alpha + \alpha\beta)\mathbf{e}_i = \mathcal{B}\mathbf{e}_i$ for any $\beta \in (-1, 1)$, applying the reverse triangle inequality, and writing the Hessian of \tilde{R} as $\mathcal{H}_{\tilde{R}}(\alpha)$ yields

$$|\tilde{S}_i(\alpha + \alpha\beta) - \tilde{S}_i(\alpha)| \leq \left\| \mathcal{P}(\mathcal{H} + \mathcal{H}_{\tilde{R}}(\alpha(1 + \beta)))^{-1}\mathcal{B}\mathbf{e}_i - \mathcal{P}(\mathcal{H} + \mathcal{H}_{\tilde{R}}(\alpha))^{-1}\mathcal{B}\mathbf{e}_i \right\|_{W_Z}.$$

Following the same arguments as in the proof of Theorem 4.4 with the Sherman-Morrison formula for rank one updates and properties of norms we have

$$\frac{|\tilde{S}_i(\alpha + \alpha\beta) - \tilde{S}_i(\alpha)|}{\|\mathcal{H}^{-1}\mathcal{B}\mathbf{e}_i\|_{W_Z}} \leq \left| \frac{1}{\alpha + \mathbf{s}^T\mathbf{n}} - \frac{1}{\alpha(1 + \beta) + \mathbf{s}^T\mathbf{n}} \right| \cdot \frac{1}{\|\mathbf{g}\|_2} \cdot \|\mathcal{P}\mathcal{H}^{-1}\mathbf{g}\mathbf{g}^T\|_{W_Z}$$

Then $\|\mathcal{P}\mathcal{H}^{-1}\mathbf{g}\mathbf{g}^T\|_{W_Z} = \|\mathbf{g}\|_2 \cdot \|\mathcal{P}\mathbf{n}\|_{W_Z}$ since $\|\mathcal{P}\mathcal{H}^{-1}\mathbf{s}\mathbf{s}^T\|_{W_Z} = \|\mathcal{P}\mathcal{H}^{-1}\mathbf{s}\|_{W_Z}$.

Hence,

$$\frac{|\tilde{S}_i(\alpha + \alpha\beta) - \tilde{S}_i(\alpha)|}{\|\mathcal{H}^{-1}\mathcal{B}\mathbf{e}_i\|_{W_Z}} \leq \left| \frac{1}{\alpha + \mathbf{s}^T\mathbf{n}} - \frac{1}{\alpha(1 + \beta) + \mathbf{s}^T\mathbf{n}} \right| \|\mathcal{P}\mathbf{n}\|_{W_Z}.$$

Algebraic manipulations give

$$\frac{|\tilde{S}_i(\alpha + \alpha\beta) - \tilde{S}_i(\alpha)|}{\|\mathcal{H}^{-1}\mathcal{B}\mathbf{e}_i\|_{W_Z}} \leq |\beta| \cdot \frac{\alpha\|\mathcal{P}\mathbf{n}\|_{W_Z}}{(\alpha + \mathbf{s}^T\mathbf{n})(\alpha(1 + \beta) + \mathbf{s}^T\mathbf{n})}.$$

Noting that $\mathbf{s}^T\mathbf{n} > 0$ so $\alpha/(\alpha + \mathbf{s}^T\mathbf{n}) < 1$ completes the proof. \square

Theorem 4.5 states that for perturbations of α in the form $\alpha(1 + \beta)$ for $\beta \in (-1, 1)$, changes in the hyper-differential sensitivities are proportional to $|\beta|$, the relative change in α , times a constant proportional to $\|\mathcal{P}\mathbf{n}\|$, which is generally small since \mathcal{P} projects on the likelihood informed subspace. This ensures that inferences drawn from HDSA are robust with respect to the length scale parameter α .

4.3. Second order a posteriori update. The first order a posteriori update \tilde{R} developed in subsection 4.2 addresses the theoretical challenge posed by failing to meet the first order optimality condition $\nabla_{\mathbf{z}} J(\mathbf{z}^*; \boldsymbol{\theta}_{\text{prior}}) = 0$. In this subsection, we address the theoretical challenge posed by failing to meet the second order optimality condition that $\mathcal{H} = \nabla_{\mathbf{z}, \mathbf{z}} J(\mathbf{z}^*; \boldsymbol{\theta}_{\text{prior}})$ is positive definite. This may occur in nonlinear inverse problems where \mathcal{H} has eigenvalues which are negative but small in magnitude, for instance, as a result of specifying a weak prior and terminating the optimization routine prematurely because of ill-conditioning and slow convergence. We propose to overcome this theoretical limitation with another prior perturbation which we call the second order update.

Rather than posing an optimization problem to determine the second order update (as was done in (4.5) for the first order update), we consider the expression (4.4) for the LIS-hyper-differential sensitivity indices in Theorem 4.1 and seek to define an update which ensures that \mathcal{H} is positive definite while not effecting the terms in (4.4), i.e. the eigenvalues and eigenvectors defining the likelihood informed subspace. This will provide a theoretical basis to justify the sensitivity indices but will not require any explicit computation of the update.

Theorem 4.6 characterizes the Hessian's positive definiteness in terms of the generalized eigenvalues which define the likelihood informed subspace.

THEOREM 4.6. *Let $\mathcal{H}_M, \mathcal{H}_R \in \mathbb{R}^{m \times m}$ be symmetric matrices and \mathcal{H}_R be positive definite. Then $\mathcal{H}_M + \mathcal{H}_R$ is positive definite if and only if the generalized eigenvalues of $(\mathcal{H}_M, \mathcal{H}_R)$ are greater than -1, i.e. $\mathcal{H}_M \mathbf{v}_j = \lambda_j \mathcal{H}_R \mathbf{v}_j$ with $\lambda_j > -1 \forall j$.*

Proof. (\rightarrow) Assume that $\mathcal{H}_M + \mathcal{H}_R$ is positive definite and let $\mathcal{H}_M \mathbf{v}_j = \lambda_j \mathcal{H}_R \mathbf{v}_j$, $j = 1, 2, \dots, m$. Without loss of generality, assume that $\mathbf{v}_j^T \mathcal{H}_R \mathbf{v}_j = 1$, $j = 1, 2, \dots, m$. Then $0 < \mathbf{v}_j^T (\mathcal{H}_M + \mathcal{H}_R) \mathbf{v}_j = \mathbf{v}_j^T (\lambda_j \mathcal{H}_R \mathbf{v}_j + \mathcal{H}_R \mathbf{v}_j) = (\lambda_j + 1) \mathbf{v}_j^T \mathcal{H}_R \mathbf{v}_j = \lambda_j + 1$. (\leftarrow) Assume that $\mathcal{H}_M \mathbf{v}_j = \lambda_j \mathcal{H}_R \mathbf{v}_j$ with $\lambda_j > -1$, $j = 1, 2, \dots, m$. Let $\mathbf{x} \in \mathbb{R}^m$, $\mathbf{x} \neq 0$. It is sufficient to show that $\mathbf{x}^T (\mathcal{H}_M + \mathcal{H}_R) \mathbf{x} > 0$. Since $\{\mathbf{v}_j\}_{j=1}^m$ forms a \mathcal{H}_R orthonormal basis for \mathbb{R}^m we can write $\mathbf{x} = \sum_{j=1}^m (\mathbf{x}^T \mathcal{H}_R \mathbf{v}_j) \mathbf{v}_j$. Then we have

$$\begin{aligned}
\mathbf{x}^T (\mathcal{H}_M + \mathcal{H}_R) \mathbf{x} &= \left(\sum_{j=1}^m (\mathbf{x}^T \mathcal{H}_R \mathbf{v}_j) \mathbf{v}_j \right)^T (\mathcal{H}_M + \mathcal{H}_R) \left(\sum_{k=1}^m (\mathbf{x}^T \mathcal{H}_R \mathbf{v}_k) \mathbf{v}_k \right) \\
&= \left(\sum_{j=1}^m (\mathbf{x}^T \mathcal{H}_R \mathbf{v}_j) \mathbf{v}_j \right)^T \left(\sum_{k=1}^m (\mathbf{x}^T \mathcal{H}_R \mathbf{v}_k) (\mathcal{H}_M \mathbf{v}_k + \mathcal{H}_R \mathbf{v}_k) \right) \\
&= \left(\sum_{j=1}^m (\mathbf{x}^T \mathcal{H}_R \mathbf{v}_j) \mathbf{v}_j \right)^T \left(\sum_{k=1}^m (\mathbf{x}^T \mathcal{H}_R \mathbf{v}_k) (\lambda_k + 1) \mathcal{H}_R \mathbf{v}_k \right) \\
&= \sum_{j=1}^m (\mathbf{x}^T \mathcal{H}_R \mathbf{v}_j)^2 (\lambda_j + 1) \\
&> 0
\end{aligned}$$

since $\lambda_j + 1 > 0$ for all $j = 1, 2, \dots, m$. \square

Adding an update in the directions of the generalized eigenvectors whose corresponding eigenvalues are less than -1 ensure positive definiteness of the Hessian. This update is characterized in Theorem 4.7.

THEOREM 4.7. *Let $\mathcal{H}_M, \mathcal{H}_R \in \mathbb{R}^{m \times m}$ be symmetric matrices and \mathcal{H}_R be positive definite. Assume that $\mathcal{H}_M \mathbf{v}_j = \lambda_j \mathcal{H}_R \mathbf{v}_j$ and $\mathbf{v}_j^T \mathcal{H}_R \mathbf{v}_j = 1$, $j = 1, 2, \dots, m$. Define the update $\mathcal{U} = \delta \mathcal{H}_R \mathbf{v}_m \mathbf{v}_m^T \mathcal{H}_R$. Then $(\mathcal{H}_M + \mathcal{U}) \mathbf{v}_j = \lambda_j \mathcal{H}_R \mathbf{v}_j$, $j = 1, 2, \dots, m - 1$ and $(\mathcal{H}_M + \mathcal{U}) \mathbf{v}_m = (\lambda_m + \delta) \mathcal{H}_R \mathbf{v}_m$.*

Proof. Let $j \in \{1, 2, \dots, m - 1\}$. Then

$$(\mathcal{H}_M + \mathcal{U}) \mathbf{v}_j = \mathcal{H}_M \mathbf{v}_j + \delta \mathcal{H}_R \mathbf{v}_m \mathbf{v}_m^T \mathcal{H}_R \mathbf{v}_j = \lambda_j \mathcal{H}_R \mathbf{v}_j + \delta \mathcal{H}_R \mathbf{v}_m(0) = \lambda_j \mathcal{H}_R \mathbf{v}_j$$

since $\{\mathbf{v}_j\}_{j=1}^m$ are \mathcal{H}_R orthogonal (a consequence of the spectral theorem for symmetric matrices). As for \mathbf{v}_m , consider

$$(\mathcal{H}_M + \mathcal{U}) \mathbf{v}_m = \mathcal{H}_M \mathbf{v}_m + \delta \mathcal{H}_R \mathbf{v}_m \mathbf{v}_m^T \mathcal{H}_R \mathbf{v}_m = \lambda_m \mathcal{H}_R \mathbf{v}_m + \delta \mathcal{H}_R \mathbf{v}_m(1) = (\lambda_m + \delta) \mathcal{H}_R \mathbf{v}_m.$$

\square

Theorems 4.6 and 4.7 suggest that when

$$\lambda_1 \geq \lambda_2 \geq \dots \geq \lambda_K > -1 \geq \lambda_{K+1} \geq \dots \geq \lambda_m,$$

we define the second order update

$$\tilde{\tilde{R}}(\mathbf{z}) = \frac{1}{2} \sum_{i=K+1}^m (\mathbf{z} - \mathbf{z}^*)^T \mathcal{U}_i (\mathbf{z} - \mathbf{z}^*)$$

where

$$\mathcal{U}_i = (-1 - \lambda_i + \epsilon) \mathcal{H}_R \mathbf{v}_i (\mathcal{H}_R \mathbf{v}_i)^T$$

for an arbitrarily small $\epsilon > 0$. Adding $\tilde{\tilde{R}}(\mathbf{z})$ to \tilde{J} ensures that the second order optimality condition is satisfied at \mathbf{z}^* .

The generalized eigenvalues less than -1 correspond to directions where the misfit has small negative curvature and the regularization (which is convex) has positive curvature which is smaller in magnitude. This occurs in directions that are not informed by data and hence are not in the range of \mathcal{P} . As Theorem 4.7 demonstrates, an update in these directions does not change the leading generalized eigenvectors and hence does not change the LIS-hyper-differential sensitivity indices. Since the update only effects the generalized eigenvectors in the uninformed directions it is not necessary to explicitly compute them. This theoretical development serves to justify HDSA when the second order optimality condition is not satisfied but does not require additional computation.

A result analogous to Theorem 4.3 may be shown for the second order update. In particular, that the perturbed prior PDF from the second order update has its mean shifted and its covariance reduced in the direction of $\Gamma_{\text{prior}} \mathcal{H}_R \mathbf{v}_i$, for each $\lambda_i \leq -1$. This reduction in uncertainty strengthens the prior in the direction $\Gamma_{\text{prior}} \mathcal{H}_R \mathbf{v}_i$, which is equivalent to increasing the regularization in this direction, thus ensuring positive definiteness of the Hessian.

EXAMPLE 4.8. To illustrate ideas presented in this section, consider the linear parameter-to-observable map

$$F(z_1, z_2) = z_1 + z_2.$$

Assume that data is generated by evaluating F at a “true” parameter $(2, -1)$ and contaminated with additive noise. Assuming a Gaussian noise model and Gaussian prior for \mathbf{z} with mean $\mathbf{z}_{\text{prior}} = (0, 0)$ and covariance matrix $\Gamma_{\text{prior}} = 3^2 I$, the negative log of the (unnormalized) posterior PDF is given by

$$(4.9) \quad J(z_1, z_2) = \frac{1}{2} \frac{(z_1 + z_2 - 1.101)^2}{.01} + \frac{1}{2} \frac{z_1^2 + z_2^2}{9}.$$

The parameter-to-observable map is constant along the line $z_1 = -z_2$ and hence the data cannot inform the posterior in this direction. Assume that \mathbf{z}^* is an approximation of the MAP point \mathbf{z}_{MAP} which differs by a perturbation in this uninformed direction. Though the MAP point may be easily determined in this simple problem, it serves as a prototypical case emulating a common challenge in large-scale inverse problems.

To illustrate likelihood informed subspaces and the first order update, Figure 2 displays the objective function J and first order update \tilde{R} . The plots are overlaid with a cyan arrow pointing in the direction of the likelihood informed subspace (the leading generalized eigenvector) and a red arrow pointing in the direction of the uninformed subspace (the trailing generalized eigenvector). Observe that J varies in the direction of the informed subspace and is flat in the direction of the uninformed subspace, while \tilde{R} is the opposite.

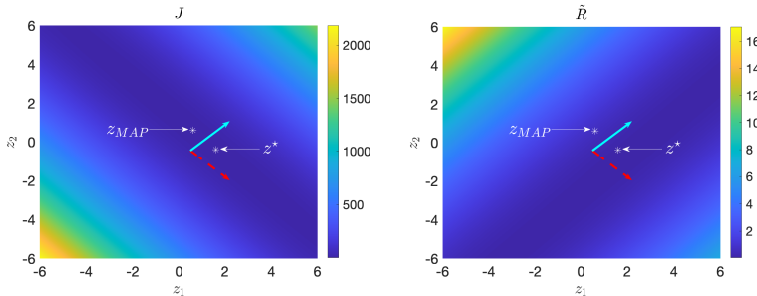


FIG. 2. Objective function J (left) and first order update \tilde{R} (right). The solid cyan arrow indicates the likelihood informed subspace and the broken red arrow indicates the uninformed subspace.

To further illustrate the first order update, Figure 3 displays the prior PDF and the update prior PDF (given by Theorem 4.3). The direction of the update $\mathbf{v} = \Gamma_{\text{prior}} \mathbf{g}$ is indicated by the magenta arrow. The updated prior highlights Theorem 4.3 which indicates that the mean is shifted and the uncertainty is reduced in the direction of \mathbf{v} .

5. Algorithmic overview. The developments of Section 4 are encapsulated to provide a concise perspective on the computational components of our proposed LIS-HDSA. Algorithm 5.1 outlines the computations required. Line 1 solves a PDE-constrained optimization problem to estimate the MAP point. Lines 2 and 3 are the computational steps required for LIS-HDSA, and Line 4 is a simple postprocessing of the data from Lines 2 and 3 to compute the sensitivities. The subsections below expand on Lines 2 and 3 of Algorithm 5.1.

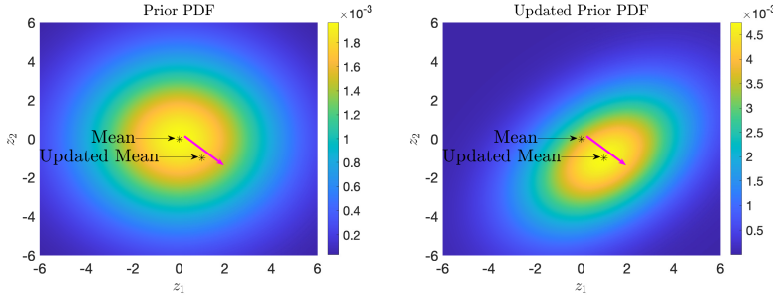


FIG. 3. Comparison of the prior PDF (left) and the update prior PDF (right). The magenta arrow indicates the direction of $\mathbf{v} = \Gamma_{\text{prior}}\mathbf{g}$.

The computational cost is dominated by the PDE solves required to compute matrix-vector products with \mathcal{H}_M in Line 2 and with \mathcal{B} in Line 3. The cost of the first order update is negligible and the second order update is a strictly theoretical tool and does not require computation. Note that Line 2 uses the updated regularization $\mathcal{H}_R + \mathcal{H}_{\bar{R}}$ rather than \mathcal{H}_R which was presented in (4.1). This is because the likelihood informed subspace was presented before the a posteriori updates in Section 4 for clarity of the exposition, but it assumes satisfaction of the optimality conditions which requires that the a posteriori updates have already been added.

Algorithm 5.1 Computation of LIS-hyper-differential sensitivity indices

- 1: Solve the MAP point estimation problem (possibly with early termination)

$$\min_{\mathbf{z} \in \mathbb{R}^m} J(\mathbf{z}, \boldsymbol{\theta}_{\text{prior}}) := M(\mathbf{z}, \boldsymbol{\theta}_{\text{prior}}) + R(\mathbf{z})$$

- 2: Compute the leading eigenpairs of $\mathcal{H}_M \mathbf{v}_j = \lambda_j (\mathcal{H}_R + \mathcal{H}_{\bar{R}}) \mathbf{v}_j$, $j = 1, 2, \dots, r$
 - 3: Compute $\mathcal{B} e_i = \nabla_{\mathbf{z}, \boldsymbol{\theta}} J(\mathbf{z}^*; \boldsymbol{\theta}_{\text{prior}}) e_i$, $i = 1, 2, \dots, n$
 - 4: Compute the hyper-differential sensitivity indices using (4.4)
-

5.1. Hessian generalized eigenvalue problem. In general, the misfit Hessian is only accessible via matrix-vector products so the Hessian generalized eigenvalue problem (GEVP), Line 2 of Algorithm 5.1, may be solved with either iterative methods (such as Krylov solvers) or randomized methods. Each matrix-vector product with the misfit Hessian requires two PDE solves (assuming that adjoints are used [30]). Randomized methods afford greater parallelism than iterative methods when adequate computational resources are available [16, 27]. Algorithm 5.2 adapts Algorithm 6 in [28] and provides a scalable (in inversion parameter dimension) approach to solve the Hessian GEVP by iterating on the number of desired eigenvalues (defined by the while loop at Line 5 of Algorithm 5.2) whose termination criteria comes from the interpretation of the eigenvalues as a ratio of contributions from the likelihood and prior (4.2).

The randomized GEVP algorithm sketches the range space of $(\mathcal{H}_R + \mathcal{H}_{\bar{R}})^{-1} \mathcal{H}_M \in \mathbb{R}^{m \times m}$ by applying it to a collection of independent random vectors. This sketch defines a low dimensional subspace which \mathcal{H}_M is projected onto to define a small dense matrix whose eigenvalues and eigenvectors may be computed through direct methods and used to approximate the leading generalized eigenvalues and eigenvectors of

Algorithm 5.2 Randomized Generalized Hermitian Eigenvalue Algorithm

-
- 1: **Input:** oversampling factor $p \in \mathbb{N}$, initial target rank $r_0 \in \mathbb{N}$, rank increment $\Delta r \in \mathbb{N}$, minimum eigenvalue threshold $\lambda_{min} \in \mathbb{R}$
 - 2: Set $\lambda_{iter} = \infty$
 - 3: Set $r = r_0$
 - 4: Generate a random matrix $\Omega \in \mathbb{R}^{n \times (r_0 + p)}$
 - 5: **while** $\lambda_{iter} > \lambda_{min}$ **do**
 - 6: **if** Number of Columns of $\Omega < r + p$ **then**
 - 7: $\Omega = [\Omega, \Omega_{\Delta r}]$ for a randomly generated $\Omega_{\Delta r} \in \mathbb{R}^{n \times \Delta r}$
 - 8: Set $r = r + \Delta r$
 - 9: **end if**
 - 10: Compute $Y = (\mathcal{H}_R + \mathcal{H}_{\bar{R}})^{-1} \mathcal{H}_M \Omega$
 - 11: Compute Q , whose columns span the range of Y , with $Q^T (\mathcal{H}_R + \mathcal{H}_{\bar{R}}) Q = I$
 - 12: Compute $T = Q^T \mathcal{H}_M Q$
 - 13: Compute the eigen decomposition $T = S \Lambda S^T$ (with decreasing eigenvalues on the diagonal of Λ)
 - 14: Set $\lambda_{iter} = (\Lambda)_{r,r}$ (the r^{th} eigenvalue in Λ)
 - 15: **end while**
 - 16: Compute $\mathbf{v}_j = Q \mathbf{s}_j$, $j = 1, 2, \dots, r$, where \mathbf{s}_i is the j^{th} column of S (normalized so that $\mathbf{v}_j^T (\mathcal{H}_R + \mathcal{H}_{\bar{R}}) \mathbf{v}_j = 1$)
 - 17: **Return:** Estimated generalized eigenvalues and eigenvectors $\{\lambda_j, \mathbf{v}_j\}_{j=1}^r$
-

$(\mathcal{H}_M, \mathcal{H}_R + \mathcal{H}_{\bar{R}})$. The accuracy of randomized solvers for a given number of matrix-vector products is slightly poorer (though in many cases not by much) than a Krylov method with a comparable number of matrix-vector products; however, the randomized algorithm allows a reordering of computation to execute matrix-vector products simultaneously rather than sequentially; which yields improved wall clock time performance when sufficient computing resources are available.

With high probability, the sketch $(\mathcal{H}_R + \mathcal{H}_{\bar{R}})^{-1} \mathcal{H}_M \Omega$ defines a $r + p$ dimensional subspace. The input p (oversampling factor) ensures that the subspace defined by the leading r eigenvectors is well approximated by this $r + p$ dimensional subspace. The oversampling factor is well understood and is typically taken to be on the order of 10-20 [15, 28] to give an accurate approximation of the leading eigenvectors with high probability. Since the generalized eigenvalues appear in the denominator in (4.4), and the smallest generalized eigenvalues/vectors are the hardest to estimate, we suggest taking $p = 20$ to ensure reliable computation.

Assuming that L processors are available to execute Algorithm 5.2 (or L subsets of processors where each subset executes a parallel PDE solve), the inputs r_0 and Δr should be taken as $r_0 = L - p$ and $\Delta r = L$ to enable all matrix-vector products (applying \mathcal{H}_M columns of Ω) in Lines 10 and 12 to be executed simultaneously.

The while loop terminates on a minimum eigenvalue threshold λ_{min} which the user chooses a priori using the interpretation of the eigenvalues (4.2). Setting $\lambda_{min} = 1$ projects on the subspace where the likelihood contributes more than the prior. A different value of λ_{min} may be more appropriate for any given application.

Since there is some ambiguity in the choice of λ_{min} we propose an approach to assess the robustness of the sensitivity indices with respect to changes in λ_{min} . Specifically, the user may execute Algorithm 5.2 with λ_{min} less than their desired threshold. The LIS-hyper-differential sensitivities may be computed via (4.4) for

different choices of r (corresponding to different eigenvalue thresholds) at a negligible computational cost. We demonstrate this in Section 6.

The computational cost of the Algorithm 5.2 is dominated by the products involving \mathcal{H}_M in Lines 10 and 12. These lines may reuse matrix-vector products from previous iterations of the while loop so the total number of matrix-vector products involving \mathcal{H}_M is $2(r+p)$, where r is the target rank at the termination of the while loop. Lines 10 and 12 are embarrassingly parallel due to the randomization decoupling the vectors, hence the cost is mitigated when computational resources are available to parallelize.

The random matrix generation in Lines 4 and 7 may be done in a variety of ways but most commonly have entries sampled independently from a standard normal distribution. The orthogonalization in Line 11 may be done with a combinations of Cholesky and QR matrix decompositions, see Algorithms 4 and 5 in [28] for details. The eigen decomposition in Line 13 is on a small dense matrix and may be done using classical dense linear algebra kernels.

5.2. Action of \mathcal{B} . If $\{\mathcal{B}e_i\}_{i=1}^n$ are computed directly, the computational cost for Line 3 of Algorithm 5.1 is $2n$ PDE solves [30] (n is the dimension of the auxiliary parameters θ). For moderate n , this cost is easily mitigated by parallelism of the matrix-vector products (it is embarrassingly parallel for up to n processors). For large values of n , which is common when auxiliary parameters are spatially or temporally distributed, Line 3 becomes computationally intensive. However, when n is large there is frequently low rank structure in the auxiliary parameter space which may be exploited by computing its Singular Value Decomposition. This has the potential to significantly reduce the number of matrix-vector products.

6. Numerical results. This section demonstrates the use of LIS-HDSA for a tracer test permeability inversion. This example is prototypical of inverse problems characterized by nonlinear physics and spatially sparse data which produces ill-posedness. Permeability inversion, though challenging for aforementioned reasons, is critical in fields such as ground water management and petroleum reservoir characterization. This prototypical inverse problem emulates many characteristics of more complex material property estimation and source identification problems.

6.1. Inverse problem formulation. We consider inverting for a log permeability field κ via a tracer test. Specifically, we use observations of the tracer concentration c and fluid pressure p which are modeled (in two dimensions) by the advection diffusion equation and Darcy's equation, respectively. Taking a mean zero Gaussian prior whose covariance matrix is given by the inverse of the weak form of the elliptic operator $-\gamma_1\Delta + \gamma_2I$ equipped with zero Neumann boundary conditions, and a Gaussian noise model with covariance matrix given by a block diagonal matrix corresponding to concentration and pressure measurements, the MAP point(s) of the posterior distribution are computed by solving

$$(6.1) \quad \min_{\kappa} \sum_{i=1}^{n_c} w_c (\mathcal{T}_c^i c(\kappa) - d_c^i)^2 + \sum_{i=1}^{n_p} w_p (\mathcal{T}_p^i p(\kappa) - d_p^i)^2 + \gamma_1 \|\nabla \kappa\|^2 + \gamma_2 \|\kappa\|^2$$

where \mathcal{T}_c^i and \mathcal{T}_p^i denote observation operators (depicted in Figure 4), d_c^i and d_p^i denotes the observed (noisy) data for concentration and pressure, and $(c(\kappa), p(\kappa))$

satisfy the system of PDEs

$$\begin{aligned}
-\nabla \cdot (e^\kappa \nabla p) &= 0 && \text{in } D \\
\frac{\partial c}{\partial t} - \nabla \cdot (\epsilon(\boldsymbol{\theta}) \nabla c) + \nabla \cdot (-e^\kappa \nabla p c) &= g(\boldsymbol{\theta}) && \text{in } [0, T] \times D \\
p &= p_1(\boldsymbol{\theta}) && \text{on } \Gamma_1 \\
p &= p_2(\boldsymbol{\theta}) && \text{on } \Gamma_3 \\
e^\kappa \nabla p \cdot \mathbf{n} &= 0 && \text{on } \Gamma_0 \cup \Gamma_2 \\
\nabla c \cdot \mathbf{n} &= 0 && \text{on } [0, T] \times \{\Gamma_0 \cup \Gamma_1 \cup \Gamma_2 \cup \Gamma_3\} \\
c(0, x) &= 0 && \text{in } D
\end{aligned}$$

on the domain $D = (0, 1)^2$ with Γ_i , $i = 0, 1, 2, 3$, denoting the four sides of the square (depicted in Figure 4).

The PDE constraint depends on the pressure Dirichlet conditions

$$p_1(\boldsymbol{\theta}) = (15 + \cos(2\pi y) + .5 \cos(4\pi y)) \delta_{p_1}(\boldsymbol{\theta}) \quad \text{and} \quad p_2(\boldsymbol{\theta}) = (10 + 2 \cos(2\pi y)) \delta_{p_2}(\boldsymbol{\theta})$$

where

$$\delta_{p_i}(\boldsymbol{\theta}) = 1 + 0.1 \sum_{j=1}^N \theta_{((i-1)N+j)} \phi_j, \quad i = 1, 2,$$

are parameterized perturbations such that $p_1(0)$ and $p_2(0)$ corresponds to a best estimate of the boundary conditions with their uncertainty parameterized by $\boldsymbol{\theta}$, where $\{\phi_j\}_{j=1}^N$ are linear finite element basis functions defined on $[0, 1]$. The tracer source is described by

$$g(\boldsymbol{\theta}) = \sum_{k=1}^{16} 10e^{-100((x-v_k)^2+(y-w_k)^2)} \delta_{s_k}(\boldsymbol{\theta})$$

where the source injection locations (v_k, w_k) are arranged in a 4×4 grid as depicted by the diamonds in Figure 4 and

$$\delta_{s_k}(\boldsymbol{\theta}) = 1 + 0.1 \sum_{j=1}^9 \theta_{(2N+(k-1)9+j)} \psi_j, \quad k = 1, 2, \dots, 16,$$

are perturbations parameterizing mechanical uncertainty in the tracer injection, where $\{\psi_j\}_{j=1}^9$ denote linear finite element basis functions defined on a 3×3 square mesh centered at the source injections. The diffusion coefficient is given by $\epsilon(\boldsymbol{\theta}) = .025(1 + 0.1\theta_{(2N+145)})$. Using $N = 21$, this yields 187 auxiliary parameters representing uncertainty in the PDEs with $\boldsymbol{\theta}_{\text{prior}} = \mathbf{0} \in \mathbb{R}^{187}$ corresponding to our best estimate which is fixed when estimating the log permeability MAP point.

To avoid the inverse crime, we generate data by solving the forward problem on a 128×128 rectangular mesh with 151 time steps, add zero-mean Gaussian white noise whose standard deviation is 1% of the observation, and sparsify in space (the observation locations are depicted in Figure 4). The optimization problem is solved on a 64×64 rectangular mesh with 76 time steps (halving the discretization in both space and time). For both the data generation and the inverse problem we set the final time $T = 0.25$.

The weights parameterizing the prior are $\gamma_1 = 10^{-5}$ and $\gamma_2 = 10^{-8}$. The weights in the noise covariance, w_c and w_p , normalize the misfit so that each data point

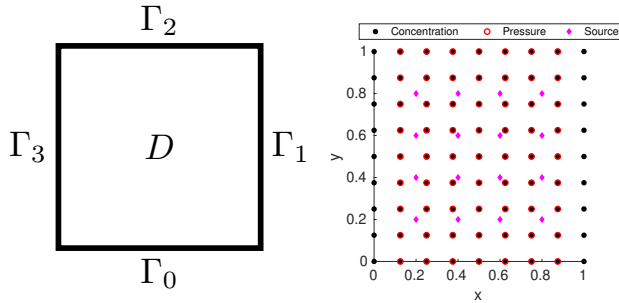


FIG. 4. *Left: schematic of the computational domain and boundaries; right: locations of concentration sensors (dots), pressure sensors (circles), and source injection sites (diamonds). The concentration and pressure sensors overlap with the exception of pressure sensors excluded from the pressure Dirichlet boundaries.*

is comparable. The discretized log permeability field κ is denoted by $\mathbf{z} \in \mathbb{R}^{4225}$ and the concatenation of discretized pressure and concentration states is denoted by $\mathbf{u} \in \mathbb{R}^{325325}$.

6.2. MAP point estimation. A MAP point is computed with $\boldsymbol{\theta} = \mathbf{0}$ using a truncated conjugate gradient trust region algorithm with 125 iterations. Table 1 displays the iteration history. The slow convergence observed in this example is typical for large-scale nonlinear inverse problems. Comparing the solutions after 75 iterations and 125 iterations shows that the quality of the estimate is not notably different, despite the fact that it took significantly more computation time to run these 50 iterations. Further, based on the trends in Table 1, it may take many additional iterations to convergence which equates to significant wall clock time in unnecessary computation. This challenge exemplifies our motivation to apply HDSA to suboptimal solutions rather than requiring convergence to justify the analysis.

Iteration	Objective	Gradient Norm	Step Size
0	17.2	1.33	N/A
4	9.59	.697	15.6
10	3.29	.676	2.38
41	.897	.113	2.02
65	.578	.331	.115
75	.571	.102	.109
125	.529	.081	.034

TABLE 1
Iteration history for MAP point estimation.

The initial iterate, estimated log permeability field (MAP point), and the “true” log permeability field which generated the data are given in Figure 5. We observe that the high and low permeability regions in the middle of the domain are apparent in the MAP point, while many of the fine scale features are not resolved. This is unsurprising given the diffusivity and nonlinearity of the physics.

Figure 6 displays (top row) the pressure and time snapshots of the concentration computed using the estimated log permeability field alongside (bottom row) the corresponding data, $\{d_c^i, d_p^i\}$, plotted as a field rather than sparse data. The pressure Dirichlet conditions induce a flow from right to left. As a result of the high

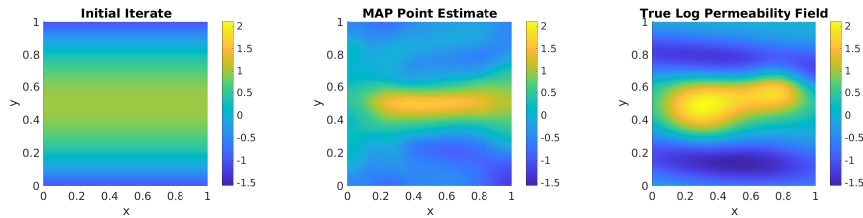


FIG. 5. *Left: initial iterate for the inverse problem; center: estimated log permeability field; right: true log permeability field used to generate the data.*

permeability region around $y = 0.5$, the tracer, which enters the domains through sixteen injection sites, is advected toward two outflow regions around $(0, 0.4)$ and $(0, 0.6)$. The regions of greatest estimation error in Figure 5 are unsurprising given the characteristics of the flow in Figure 6. Comparing the good fit of the state data in Figure 6 with the log permeability field error in Figure 5 highlights the ill-posedness of the problem, a characteristic commonly observed in practice.

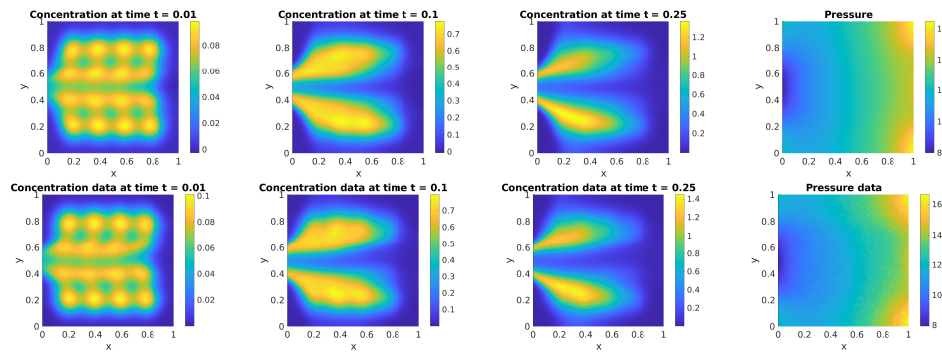


FIG. 6. *Pressure and time snapshots of concentration. The top row is computed by using the estimated log permeability field (center panel of Figure 5) while the bottom row is computed by using the true log permeability field (right panel of Figure 5) and adding noise. From left to right displays the time evolution of the concentration with the pressure in the rightmost panel.*

Traditional Bayesian inference methods such as Markov Chain Monte Carlo sampling or a Laplace approximation of the posterior covariance could be considered to identify the regions of the log permeability field which are most uncertain (rightmost region of the domain in our example). However, these approaches do not directly address the uncertainty in log permeability field created by uncertainty in θ . We address this question with our proposed HDSA algorithm. Assessing local correlations with HDSA provides insights which are complementary to other Bayesian inference approaches.

6.3. HDSA results. There is no theoretical justification to use HDSA on this inverse problem without the developments of Section 4. The MAP point estimation only reduces the gradient norm by two orders of magnitude despite significant computational efforts, and the Hessian is indefinite due to insufficient information in the prior. This serves as an illustrative and motivating application for the contributions of this article.

We compute hyper-differential sensitivity indices using Algorithms 5.1 and 5.2. To explore the choice of eigenvalue threshold, Algorithm 5.2 is executed with $p = 20$,

$r_0 = 4$, $\Delta r = 8$ (the number of processors used), and $\lambda_{min} = 0.1$. This choice of λ_{min} allows us to study the robustness of the sensitivities with respect to the eigenvalue threshold.

The length scale parameter is set to $\alpha = 0.5(\max(\mathbf{z}) - \min(\mathbf{z})) = 1.4657$ as discussed in Subsection 4.2. Using Theorem 4.3, we compared samples (omitted for conciseness) from the prior and updated prior to confirm that the a posteriori update with this α introduces a negligible change in the prior. We also repeated all computation (but omitted results for conciseness) with a larger value of α to confirm that the resulting analysis is robust with respect to α .

Likelihood informed subspace and eigenvalue threshold robustness.

Figure 7 displays the generalized eigenvalues (in log scale), vertical lines indicate three possible thresholds (with the horizontal axis indicating the value of r in (4.4)). The left panel of Figure 8 shows the LIS-hyper-differential sensitivity indices (computed using (4.4)) on the vertical axis as a function of the number of generalized eigenvalues (the informed subspace dimension) on the horizontal axis. We observe that the magnitude of the largest sensitivity indices varies depending on the threshold but generally the conclusions we draw from the analysis (which parameters are most/least influential) are robust. Zooming in on the smaller sensitivity indices in the right panel of Figure 8 reveals a similar conclusion for the smallest sensitivity indices. There is some variability but the robustness conclusions of the analysis remain valid.

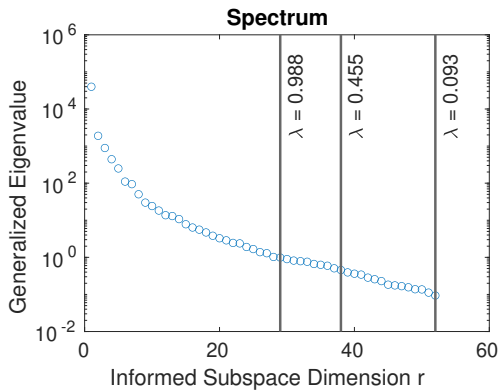


FIG. 7. Log scale plot of the generalized eigenvalues. The vertical lines indicate potential eigenvalue thresholds as a frame of reference for assessing robustness.

The spectral characteristics reveal low rank structure which is common in inverse problems. In particular, the misfit Hessian in $\mathbb{R}^{4225 \times 4225}$ is well characterized by a likelihood informed subspace of dimension $\mathcal{O}(50)$.

Bayesian interpretation of sensitivity indices. We take $\lambda_{min} = 1$ and plot the hyper-differential sensitivity indices in Figure 9 (without the scalar sensitivity index for the diffusion coefficient which equals 0.0283). Four different parameters (two pressure boundary conditions, a concentration source term, and diffusion coefficient) are easily compared in the HDSA framework. As discussed in subsection 6.2, the MAP point estimation is difficult even with these parameters fixed. Performing joint inversion on all parameters is extremely challenging and thus underscores the utility of HDSA to provide quantitative insights for complex systems with many sources of uncertainty.

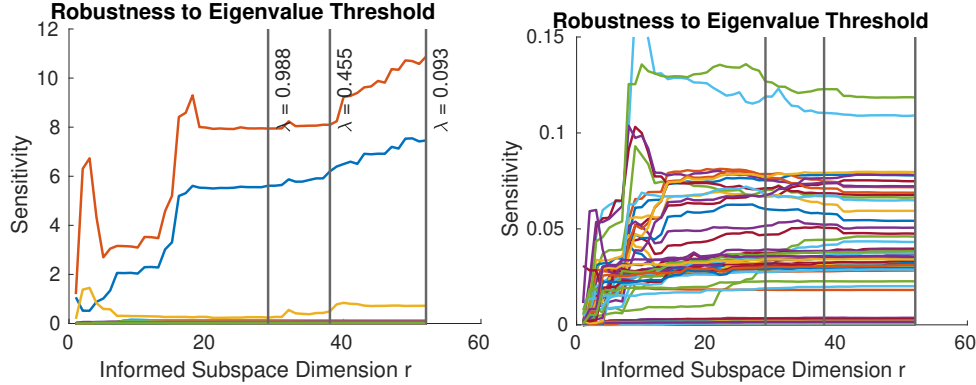


FIG. 8. *Left: dependence of the hyper-differential sensitivity indices (vertical axis) on the informed subspace dimension r (horizontal axis); right: same plot as the left but zoomed in on the smaller sensitivity indices. The vertical lines indicate potential eigenvalue thresholds as a frame of reference for assessing robustness. The curves (which are different colors to aid visualization) correspond to different sensitivity indices.*

There are two particularly large sensitivity indices near $y = 0.5$ on the $x = 1$ pressure Dirichlet boundary. Inspection of \mathcal{B} acting on the basis functions corresponding to these indices identifies this sensitivity as a large change in the estimated log permeability field in the $(1, 0.5)$ region. This result highlights the fact that the log permeability field is not well informed by the tracer in this region (the tracer is flowing away from it) and as a result the estimated log permeability field is highly dependent on the pressure data which is strongly influence by the boundary condition near $x = 1$. From a Bayesian perspective, the log permeability field and pressure boundary condition are highly correlated in the region around $(1, 0.5)$. On the $x = 0$ pressure Dirichlet boundary, we observe greater sensitivity (correlation) corresponding to the lower permeability regions as the tracer outflow is determined by the combination of the permeability and low pressure regions on the boundary. The tracer injection sensitivities are generally small, indicating that the tracer injection and log permeability field are approximately uncorrelated in their joint posterior distribution.

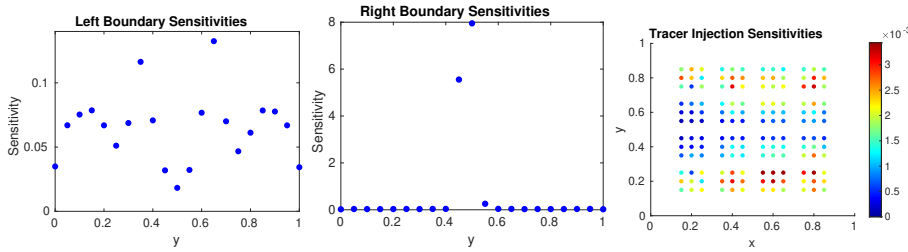


FIG. 9. *Hyper-differential sensitivity indices with $\lambda_{min} = 1$. Left: $x = 0$ pressure Dirichlet boundary condition sensitivities; center: $x = 1$ pressure Dirichlet boundary condition sensitivities; right: tracer injection sensitivities.*

The results in Figure 9 may be applied for model development, experimental design, and uncertainty quantification. The influence of the pressure Dirichlet boundary conditions indicates the importance of the pressure difference driving the flow and how the log permeability field reconstruction is dependent on the features of the

velocity field. The high sensitivity around $x = 1$ and $y = 0.5$ highlights the importance of characterizing the interaction between this region of the boundary and the log permeability field. Observing such sensitivities in practice alerts the analyst of potential concerns which may be alleviated by collecting data and/or improving modeling around the boundary.

Characterizing the covariance matrix of the posterior distribution would likely identify the uncertainty in the log permeability field near $(1.0, 0.5)$. However, understanding the correlation between the log permeability field and boundary condition would require analysis of the joint posterior distribution, a task which is particularly challenging when strong correlations (high sensitivity) exists. These strong correlations are easily identified and (locally) characterized by HDSA at a computational cost commensurate to the MAP point estimation. These insights enable goal-oriented decision-making to achieve uncertainty quantification in high dimensional parameter spaces.

7. Conclusion. Large-scale ill-posed inverse problems are challenging in many respects. Uncertainty in model parameters which are fixed (out of computational necessity) introduce uncertainty in the solution of the inverse problem which is not easily quantified in many applications. Such quantification of uncertainty may be easily formulated in a Bayesian paradigm, but complete exploration of the joint Bayesian posterior distribution for multiple parameters is challenging for problems constrained by PDEs. By introducing a Bayesian interpretation of HDSA as local correlations, we provide a means to leverage computationally scalable algorithms from PDE-constrained optimization to analyze correlations in the joint Bayesian posterior. Through a likelihood informed subspace projection and development of a posteriori updates, we have made HDSA practical for ill-posed inverse problems encountered in practice.

Exploration of the posterior uncertainty plays a critical role in many applications. For instance, correlations in the posterior, which are challenging to characterize, are vital for effective sampling in uncertainty quantification, stochastic optimization, and decision-making under uncertainty. In many applications, the ultimate end goal of an inverse problem is to properly estimate model parameters with associated uncertainty so that the model may be used to provide physical insights and direct decision-making. Incorporating HDSA in a Bayesian inversion paradigm facilitates such crucial analysis.

A key computational component is efficient Hessian vector products. Such Hessian vector products are crucial for other aspect of large-scale inverse problems [1, 26] and are topics of ongoing research. Though omitted from this article for conciseness, there are opportunities to couple the algorithmic framework for HDSA with existing approaches for Hessian based exploration of the posterior covariance.

Appendix A. Proof of the first order a posteriori update. In this appendix we derive a closed form solution to the optimization problem

$$(A.1) \quad \begin{aligned} & \min_{\tilde{R} \in Q} \|\tilde{R}\|_{L^1(\mu)} \\ & \text{s.t. } \nabla_{\mathbf{z}} \tilde{R}(\mathbf{z}^*) = -\mathbf{g} \end{aligned}$$

where Q is the set of nonnegative convex quadratic functions from \mathbb{R}^m to \mathbb{R} and $\mathbf{g} = \nabla_{\mathbf{z}} J(\mathbf{z}^*; \boldsymbol{\theta}_{\text{prior}})$.

A general expression for a function belonging to Q and satisfying $\nabla_{\mathbf{z}} \tilde{R}(\mathbf{z}^*) = -\mathbf{g}$

is given by

$$(A.2) \quad \tilde{R}(\mathbf{z}) = \frac{1}{2}(\mathbf{z} - \mathbf{z}^*)^T \mathcal{A}(\mathbf{z} - \mathbf{z}^*) - \mathbf{z}^T \mathbf{g} + C$$

where $\mathcal{A} \in \mathbb{R}^{m \times m}$ is symmetric (since it is a Hessian) positive semidefinite (to ensure non-negativity) with \mathbf{g} in the range of \mathcal{A} , and $C \in \mathbb{R}$ is chosen to ensure that \tilde{R} is non-negative. The condition that \mathbf{g} is in the range of \mathcal{A} ensures that

$$(A.3) \quad \frac{1}{2}(\mathbf{z} - \mathbf{z}^*)^T \mathcal{A}(\mathbf{z} - \mathbf{z}^*) - \mathbf{z}^T \mathbf{g}$$

is bounded below and hence a C exists which enforces $\tilde{R} \geq 0$.

To solve (A.1) we need to find a matrix \mathcal{A} and a scalar C . Since we seek to minimize the norm of \tilde{R} while enforcing $\tilde{R} \geq 0$, we express C as a function of \mathcal{A} by setting it equal to the minimum value of (A.3). Setting the gradient of (A.3) equal to zero yields the system of equations

$$\mathcal{A}(\mathbf{z}_0 - \mathbf{z}^*) = \mathbf{g}$$

which is guaranteed to admit a solution because \mathbf{g} is in the range of \mathcal{A} . Since, in general, \mathcal{A} is positive semidefinite, the set of critical points is given by $\mathbf{z}^* + \mathcal{A}^\dagger \mathbf{g} + N(\mathcal{A})$, where \mathcal{A}^\dagger denotes the pseudo-inverse of \mathcal{A} and $N(\mathcal{A})$ denotes the null space of \mathcal{A} . Plugging these critical points into (A.3) yields that the smallest C , as a function of \mathcal{A} , such that $\tilde{R} \geq 0$, is given by

$$(A.4) \quad C = \frac{1}{2} \mathbf{g}^T \mathcal{A}^\dagger \mathbf{g} + \mathbf{z}^{*T} \mathbf{g}.$$

Having written C as a function of \mathcal{A} , we may find the optimal quadratic update by minimizing over \mathcal{A} . By exploiting non-negativity of \tilde{R} to drop the absolute value in the L^1 norm, properties of the Gaussian probability measure, and ignoring terms which do not depend on \mathcal{A} , we arrive at the optimization problem

$$(A.5) \quad \begin{aligned} \min_{\mathcal{A} \in \mathcal{S}_m^+} f(\mathcal{A}) &:= \alpha^2 \text{Tr}(\mathcal{A}) + \mathbf{g}^T \mathcal{A}^\dagger \mathbf{g} \\ \text{s.t. } \mathbf{g} &\in R(\mathcal{A}) \end{aligned}$$

where \mathcal{S}_m^+ denotes the set of $m \times m$ positive semidefinite matrices with real entries and $\text{Tr}(\mathcal{A})$ denotes the trace of \mathcal{A} .

To derive a closed form expression for (A.5) (and equivalently (A.1)), we prove a sequence of lemmas to arrive at a unique solution. Using the spectral theorem for symmetric matrices we may, without loss of generality, assume that the optimal solution of (A.5) is a matrix $\mathcal{H}_{\tilde{R}}$ of the form

$$(A.6) \quad \mathcal{H}_{\tilde{R}} = \sum_{j=1}^m \lambda_j \mathbf{v}_j \mathbf{v}_j^T$$

where $\lambda_1 \geq \lambda_2 \geq \dots \geq \lambda_m \geq 0$ are the non-negative eigenvalues and $\{\mathbf{v}_j\}_{j=1}^m$ are the orthonormal eigenvectors of $\mathcal{H}_{\tilde{R}}$.

Let $r \in \{1, 2, \dots, m\}$ be the rank of $\mathcal{H}_{\tilde{R}}$. Plugging (A.6) into (A.5), writing the trace as the sum of eigenvalues, and using the spectral decomposition to express the pseudo-inverse, we find that

$$f(\mathcal{H}_{\tilde{R}}) = \alpha^2 \sum_{j=1}^r \lambda_j + \sum_{j=1}^r \frac{1}{\lambda_j} (\mathbf{g}^T \mathbf{v}_j)^2.$$

The subsequent lemmas characterize the eigenvalues $\{\lambda_j\}_{j=1}^r$ and eigenvectors $\{\mathbf{v}_j\}_{j=1}^r$ by utilizing the fact that $f(\mathcal{H}_{\bar{R}}) \leq f(\mathcal{A})$ for all $\mathcal{A} \in \mathcal{S}_m^+$ which satisfy $\mathbf{g} \in R(\mathcal{A})$.

Let λ_1 have algebraic multiplicity ℓ , i.e. $\lambda_1 = \lambda_2 = \dots = \lambda_\ell > \lambda_{\ell+1}$ (or $\lambda_j = \lambda_1$, $j = 1, 2, \dots, m$ if $\ell = m$). Then we have the following.

LEMMA A.1.

$$\mathbf{g} \in \text{span}\{\mathbf{v}_1, \mathbf{v}_2, \dots, \mathbf{v}_\ell\}.$$

Proof. We may rewrite the objective function as

$$f(\mathcal{H}_{\bar{R}}) = \alpha^2 \sum_{j=1}^r \lambda_j + \|\mathbf{g}\|_2^2 \sum_{j=1}^r \gamma_j \frac{1}{\lambda_j}$$

where $\gamma_j = (\mathbf{g}^T \mathbf{v}_j)^2 / \|\mathbf{g}\|_2^2 \in [0, 1]$ and $\sum_{i=1}^r \gamma_i = 1$ by Parseval's identity. Because of the ordering of the eigenvalues, $f(\mathcal{H}_{\bar{R}})$ is minimized when $\gamma_i = 0$ for $i > \ell$. Hence, $(\mathbf{g}^T \mathbf{v}_j) = 0$ for $j > \ell$. Since $\{\mathbf{v}_j\}_{j=1}^m$ is an orthonormal basis for \mathbb{R}^m ,

$$\mathbf{g} = \sum_{j=1}^m (\mathbf{g}^T \mathbf{v}_j) \mathbf{v}_j = \sum_{j=1}^{\ell} (\mathbf{g}^T \mathbf{v}_j) \mathbf{v}_j.$$

□

Applying Lemma A.1, we can simplify $f(\mathcal{H}_{\bar{R}})$ to get

$$(A.7) \quad f(\mathcal{H}_{\bar{R}}) = \alpha^2 \sum_{j=1}^r \lambda_j + \|\mathbf{g}\|_2^2 \frac{1}{\lambda_1}.$$

LEMMA A.2. $\lambda_j = 0$ for $j > \ell$.

Proof. The result follows by observing that all quantities in (A.7) are non-negative and it is minimized when there are a minimum number of terms in the sum of eigenvalues. □

We may now rewrite $f(\mathcal{H}_{\bar{R}})$ as

$$(A.8) \quad f(\mathcal{H}_{\bar{R}}) = \alpha^2 \ell \lambda_1 + \|\mathbf{g}\|_2^2 \frac{1}{\lambda_1}.$$

LEMMA A.3. $\ell = 1$ and $\mathbf{v}_1 = \pm \frac{\mathbf{g}}{\|\mathbf{g}\|_2}$.

Proof. Since all quantities in (A.8) are nonnegative and $\ell \in \{1, 2, \dots, m\}$, then (A.8) will be minimized when ℓ is minimized. Taking $\ell = 1$ clearly minimizes it and also implies that $\mathbf{v}_1 = \pm \frac{\mathbf{g}}{\|\mathbf{g}\|_2}$ to ensure that $\mathbf{g} \in R(\mathcal{H}_{\bar{R}})$. □

Hence, we have established that $\mathcal{H}_{\bar{R}}$ is given by the rank one matrix

$$(A.9) \quad \mathcal{H}_{\bar{R}} = \frac{\lambda}{\|\mathbf{g}\|_2^2} \mathbf{g} \mathbf{g}^T$$

where λ is the optimal eigenvalue which minimizes

$$(A.10) \quad \alpha^2 \lambda + \|\mathbf{g}\|_2^2 \frac{1}{\lambda}.$$

By setting the derivative of (A.10) with respect to λ equal to zero and solving, we find that $\mathcal{H}_{\bar{R}}$ is given by

$$(A.11) \quad \mathcal{H}_{\bar{R}} = \frac{1}{\alpha \|\mathbf{g}\|_2} \mathbf{g} \mathbf{g}^T.$$

Hence, the solution of (A.1) is (A.2) with \mathcal{A} given by (A.11) and C given by (A.4).

Acknowledgements. This paper describes objective technical results and analysis. Any subjective views or opinions that might be expressed in the paper do not necessarily represent the views of the U.S. Department of Energy or the United States Government. Sandia National Laboratories is a multimission laboratory managed and operated by National Technology and Engineering Solutions of Sandia LLC, a wholly owned subsidiary of Honeywell International, Inc., for the U.S. Department of Energy’s National Nuclear Security Administration under contract DE-NA-0003525. SAND2021-6604 O. This work was supported by the US Department of Energy, Office of Advanced Scientific Computing Research, Field Work Proposal 20-023231.

REFERENCES

- [1] I. AMBARTSUMYAN, W. BOUKARAM, T. BUI-THANH, O. GHATTAS, D. KEYES, G. STADLER, G. TURKIYYAH, AND S. ZAMPINI, *Hierarchical matrix approximations of Hessians arising in inverse problems governed by PDEs*. <https://arxiv.org/abs/2003.10173>.
- [2] H. ANTIL, D. P. KOURI, M. LACASSE, AND D. RIDZAL, eds., *Frontiers in PDE-Constrained Optimization*, Springer, 2018.
- [3] A. Y. ARAVKIN AND T. VAN LEEUWEN, *Estimating nuisance parameters in inverse problems*, *Inverse Problems*, 28 (2012).
- [4] U. M. ASCHER AND E. HABER, *Grid refinement and scaling for distributed parameter estimation problems*, *Inverse Problems*, 17 (2001), pp. 571–590.
- [5] L. BIEGLER, G. BIROS, O. GHATTAS, M. HEINKENSCHLOSS, D. KEYES, B. MALLICK, Y. MARZOUK, L. TENORIO, B. VAN BLOEMEN WAANDERS, AND K. WILLCOX, eds., *Large-Scale Inverse Problems and Quantification of Uncertainty*, John Wiley and Sons, 2011.
- [6] L. T. BIEGLER, O. GHATTAS, M. HEINKENSCHLOSS, D. KEYES, AND B. VAN BLOEMEN WAANDERS, eds., *Real-Time PDE-Constrained Optimization*, vol. 3, SIAM Computational Science and Engineering, 2007.
- [7] G. BIROS AND O. GHATTAS, *Parallel Lagrange-Newton-Krylov-Schur methods for PDE-constrained optimization. Parts I-II*, *SIAM J. Sci. Comput.*, 27 (2005), pp. 687–738.
- [8] J. F. BONNANS AND A. SHAPIRO, *Optimization problems with perturbations: A guided tour*, *SIAM Review*, 40 (1998), pp. 228–264.
- [9] A. BORZI, *High-order discretization and multigrid solution of elliptic nonlinear constrained optimal control problems*, *J. Comp. Applied Math*, 200 (2007), pp. 67–85.
- [10] T. BUI-THANH, *A gentle tutorial on statistical inversion using the Bayesian paradigm*, tech. report, The Institute for Computational Engineering and Sciences, 2012.
- [11] T. BUI-THANH, O. GHATTAS, J. MARTIN, AND G. STADLER, *A computational framework for infinite-dimensional Bayesian inverse problems. Part I: The linearized case, with applications to global seismic inversion*, *SIAM Journal on Scientific Computing*, 35 (2013), pp. A2494–A2523.
- [12] T. CUI, J. MARTIN, Y. M. MARZOUK, A. SOLONEN, AND A. SPANTINI, *Likelihood-informed dimension reduction for nonlinear inverse problems*, *Inverse Problems*, 30 (2014), pp. 1–28.
- [13] R. GRIESSE, *Parametric sensitivity analysis in optimal control of a reaction diffusion system. I. solution differentiability*, *Numerical Functional Analysis and Optimization*, 25 (2004), pp. 93–117.
- [14] E. HABER AND U. M. ASCHER, *Preconditioned all-at-once methods for large, sparse parameter estimation problems*, *Inverse Problems*, 17 (2001), pp. 1847–1864.
- [15] N. HALKO, P. G. MARTINSSON, AND J. A. TROPP, *Finding structure with randomness: Probabilistic algorithms for constructing approximate matrix decompositions*, *SIAM Review*, 53 (2011), pp. 217–288.

- [16] J. HART, B. VAN BLOEMEN WAANDERS, AND R. HERTZOG, *Hyper-differential sensitivity analysis of uncertain parameters in PDE-constrained optimization*, International Journal for Uncertainty Quantification, 10 (2020), pp. 225–248.
- [17] S. B. HAZRA AND V. SCHULZ, *Simultaneous pseudo-timestepping for aerodynamic shape optimization problems with state constraints*, SIAM J. Sci. Comput., 28 (2006), pp. 1078–1099.
- [18] M. HINTERMULLER AND L. N. VICENTE, *Space mapping for optimal control of partial differential equations*, SIAM J. Opt., 15 (2005), pp. 1002–1025.
- [19] M. HINZE, R. PINNAU, M. ULBRICH, AND S. ULBRICH, *Optimization with PDE Constraints*, Springer, 2009.
- [20] T. ISAAC, N. PETRA, G. STADLER, AND O. GHATTAS, *Scalable and efficient algorithms for the propagation of uncertainty from data through inference to prediction for large-scale problems, with application to flow of the antarctic ice sheet*, Journal of Computational Physics, 296 (2015), pp. 348–368.
- [21] J. P. KAIPIO AND E. SOMERSALO, *Statistical and Computational Inverse Problems*, Springer New York, 2005.
- [22] M. H. L. T. BIEGLER, O. GHATTAS AND B. VAN BLOEMEN WAANDERS, eds., *Large-Scale PDE-Constrained Optimization*, vol. 30, Springer-Verlag Lecture Notes in Computational Science and Engineering, 2003.
- [23] C. D. LAIRD, L. T. BIEGLER, B. VAN BLOEMEN WAANDERS, AND R. A. BARTLETT, *Time dependent contaminant source determination for municipal water networks using large scale optimization*, ASCE J. Water Res. Mgt. Plan., (2005), pp. 125–134.
- [24] T.-Z. LU AND S.-H. SHIOU, *Inverses of two block matrices*, Computers and Mathematics with Applications, (2002), pp. 119–129.
- [25] R. NICHOLSON, N. PETRA, AND J. P. KAIPIO, *Estimation of the Robin coefficient field in a Poisson problem with uncertain conductivity field*, Inverse Problems, 34 (2018).
- [26] N. PETRA, J. MARTIN, G. STADLER, AND O. GHATTAS, *A computational framework for infinite-dimensional bayesian inverse problems. Part II: Stochastic newton mcmc with application to ice sheet flow inverse problems*, SIAM Journal on Scientific Computing, 36 (2014), pp. A1525–A1555.
- [27] A. K. SAIBABA, J. HART, AND B. VAN BLOEMEN WAANDERS, *Randomized algorithms for generalized singular value decomposition with application to sensitivity analysis*, Numerical Linear Algebra with Applications, (2021), p. e2364.
- [28] A. K. SAIBABA, J. LEE, AND P. K. KITANIDIS, *Randomized algorithms for generalized Hermitian eigenvalue problems with application to computing Karhunen-Loève expansion*, Numerical Linear Algebra with Applications, 23 (2016), pp. 314–339.
- [29] A. M. STUART, *Inverse problems: a Bayesian perspective*, Acta Numerica, (2010).
- [30] I. SUNSERI, J. HART, B. VAN BLOEMEN WAANDERS, AND A. ALEXANDERIAN, *Hyper-differential sensitivity analysis for inverse problems constrained by partial differential equations*, Inverse Problems, 36 (2020).
- [31] C. R. VOGEL, *Sparse matrix computations arising in distributed parameter identification*, SIAM J. Matrix Anal. Appl., (1999), pp. 1027–1037.
- [32] C. R. VOGEL, *Computational Methods for Inverse Problems*, SIAM Frontiers in Applied Mathematics Series, 2002.